SPRINGER BRIEFS IN MOLECULAR SCIENCE
GREEN CHEMISTRY FOR SUSTAINABILITY

Antonio Arques
Alessandra Bianco Prevot *Editors*

Soluble Bio-based Substances Isolated From Urban Wastes

Environmental Applications

Springer

SpringerBriefs in Molecular Science

Green Chemistry for Sustainability

Series editor

Sanjay K. Sharma, Jaipur, India

More information about this series at http://www.springer.com/series/10045

Antonio Arques · Alessandra Bianco Prevot
Editors

Soluble Bio-based Substances Isolated From Urban Wastes

Environmental Applications

Springer

Editors
Antonio Arques
Campus de Alcoy
Universitat Politècnica de València
Alcoy
Spain

Alessandra Bianco Prevot
Università degli Studi di Torino
Torino
Italy

ISSN 2191-5407 ISSN 2191-5415 (electronic)
SpringerBriefs in Molecular Science
ISSN 2212-9898
Green Chemistry for Sustainability
ISBN 978-3-319-14743-7 ISBN 978-3-319-14744-4 (eBook)
DOI 10.1007/978-3-319-14744-4

Library of Congress Control Number: 2015930504

Springer Cham Heidelberg New York Dordrecht London

Printed on acid-free paper

Springer International Publishing AG Switzerland is part of Springer Science+Business Media (www.springer.com)

Contents

1 Soluble Bio-based Substances Obtained from Urban Wastes: Isolation and Characterization 1
A. Bianco Prevot, P. Avetta, S. Berto, P.G. Daniele, S. Tabasso, D. Mainero and E. Montoneri

2 Photogeneration of Reactive Oxygen Species by SBO and Application in Waste-Water Treatment 17
Luciano Carlos and Daniel O. Mártire

3 SBO in Water Detoxification: Photo-Fenton Processes at Mild Conditions. 29
J. Gomis, M. Mora, R. Vicente, R. Vercher, A.M. Amat and A. Arques

4 Effect of Humic Substances and Bioorganic Substrates from Urban Wastes in Nanostructured Materials Applications and Synthesis 41
G. Magnacca, E. Laurenti and M.C. Gonzalez

5 Mathematical Modeling for SBO Applications 59
A.C.S.C. Teixeira, A.M. Lastre Acosta, A.S. Vianna Jr and G.A.C. Le Roux

Introduction

The increasing environmental concern of our society has resulted in the need for developing sustainable processes able to decrease waste production or, alternatively, to valorize them for other use. This latter concept fits with the biorefinery strategy, aiming to integrate different biomass conversion approaches to obtain fuels, power, heat, and value-added chemicals from biomass. In particular, organic materials such as compost, anaerobic digestate, and organic residues from mechanical-biological treatment of urban wastes can be used as biomass to feed a biorefinery. This is the innovative idea characterizing the project "Biomass Wastes as Renewable Source of Energy and Chemicals for the Industry with Friendly Environmental Impact. Optimizing use of Piemonte wastes bioenergy inventory," financed in 2006 by the Regione Piemonte (Italy), and coordinated by the Chemistry Department of the Università di Torino (Italy). From the humid fraction of urban wastes soluble bio-organic substances (SBO) were isolated, whose chemical nature was demonstrated very similar to natural organic matter, such as humic substances. SBO show interesting physical and chemical properties, such as ability to decrease surface tension of water, photo-chemical activity under sunlight, and chelating capability for metals. Hence, SBO are good candidates to be used, in alternative to petroleum derived auxiliaries, in several fields such as textile industry, detergency, agriculture, polluted soil washing, wastewater treatment, and material chemistry. The perspective to recycle waste bio-based SBO in many processes would result in important economic and ecological advantages for industry and society. SBO are obtained from a cheap and easily available source, and their applications should be considered as green processes, as they are based on the reuse of a waste, and imply lower fossils consumption and lower concern for waste disposal.

With this background, the aim of this book is to provide information about the use of SBO for different environmental purposes. This is the basis of a project financed by the European Union in the Seventh Framework Program as a Marie Curie action and entitled "Isolation, characterization and screening of environmental applications of bio-organic substances obtained from urban biomasses," under the acronym of EnvironBOS, in which was exchanged the complementary expertise of research groups from Universidad Politécnica de Valencia

(Spain), Università degli Studi di Torino (Italy), Universidad Nacional de La Plata (Argentina), and Universidade de Sao Paulo (Brasil). The purpose of this project was to identify, among the potential applications of environmental interest, those fields where the use of SBO appears more promising for application in the real case at industrial scale, in order to focus on them in the future research. Therefore the present book witnesses the fruitful collaboration of all the researchers involved in the EnvironBOS project.

The synthesis of SBO is explained in detail in Chap. 1; their photochemical activity and ability to generate reactive species is reported in Chap. 2; Chap. 3 is devoted to report on their use in wastewater treatment, in particular as chemical auxiliaries for photo-Fenton process at mild acidic conditions; Chap. 4 reports on the synthesis and performance of different SBO-based materials, with particular attention to their application in wastewater treatment. Lastly, Chap. 5 deals with the mathematical tools to modeling and optimizing the processes involving SBO.

Acknowledgments

The authors want to thank the financial support of the European Union (PIRSES-GA-2010-269128, EnvironBOS).

Chapter 1
Soluble Bio-based Substances Obtained from Urban Wastes: Isolation and Characterization

A. Bianco Prevot, P. Avetta, S. Berto, P.G. Daniele, S. Tabasso, D. Mainero and E. Montoneri

Abstract The organic fraction of urban wastes can be considered a cost effective source of added value products for a wide number of uses. The present chapter describes different possible strategies for the treatment of organic wastes, used at the present time in many waste treatment plants. Subsequently the chapter deals with the isolation process of soluble bio-based substances (SBO) from urban biowastes at both laboratory and pilot plant scale. A detailed description of SBO composition and physical-chemical characterization is given.

Keywords Urban biowastes · Bio-based products · Aerobic digestion · Anaerobic digestion · Biosurfactants · Characterization

1.1 Introduction

Nowadays one of the most relevant global challenges is to guarantee an economic and social development environmentally sustainable. The Green chemistry policy is one of the results obtained at this purpose. The United Nations defines green growth as a policy which "emphasizes environmentally sustainable economic progress to foster low-carbon, socially inclusive development" [1].

Waste management was early recognized as an important issue for a sustainable development in the European Union (EU) and great effort is currently done to

A. Bianco Prevot (✉) · P. Avetta · S. Berto · P.G. Daniele · S. Tabasso
Dipartimento di Chimica, Università di Torino, Via P. Giuria 7, 10125 Turino, Italy
e-mail: alessandra.biancoprevot@unito.it

D. Mainero
ACEA Pinerolese Industriale SpA, Via Vigone 42, 10064 Pinerolo, Italy

E. Montoneri
STAR Integrated Research Unit, Università di Foggia, Via Gramsci 89-91, 71121 Foggia, Italy

A. Arques and A. Bianco Prevot (eds.), *Soluble Bio-based Substances Isolated From Urban Wastes*, SpringerBriefs in Green Chemistry for Sustainability,
DOI 10.1007/978-3-319-14744-4_1

Scheme 1.1 Schematic representation of the EU waste policy

optimize it. The first waste framework directive was established in 1975, followed by a number of additional directives addressing specific waste streams.

The collection, the treatment and the disposal of solid urban wastes represent one of the most relevant problems for all the developed societies and are increasing in importance also for the developing ones. Indeed, up to now, the wealth increase of a country has been closely related to an increase in waste production. To manage urban wastes has become necessary as result of increasing population urbanization and consumption habits. A sustainable green economy requires to minimize wastes and to develop an adequate waste management system able to satisfy economic, social and environmental needs.

The European regulation on waste management systems [2] indicates guidelines for the single State members, consisting mainly in reducing waste production and then in reusing, recycling and recovering materials, in order to reduce the volumes of refuses disposed in landfill facilities or burnt inside incinerators (see Scheme 1.1).

In many European cities, glass, aluminum, paper and plastic materials are separately collected or sorted from the other wastes and then recycled according to well established technologies. Paper and plastics are also burnt to recover energy.

On the contrary, the organic urban residues (for instance kitchen, fruit and garden wastes) cannot be easily exploited or recycled because they contain high amount of water and they are variable and not homogeneous in terms of composition. Although nowadays this aspect contributes to society a significant economic burden for their management and/or disposal, concentration of wastes in urban areas has in turn allowed the concentration of natural bio-organic matter in well confined spaces, allowing the envisagement of the sustainable perspective for their treatment, alternatively to landfills. At the present time, in Europe the so called landfill directive (99/31/EC) has created the fundamental push to ban organic fraction from landfill.

In the present chapter the possibility of recovering and recycling chemical energy from urban organic wastes is shown as well as the innovative approach to develop a biorefinery fed with this kind of waste in order to obtain products of potential technological and/or environmental interest.

1.2 Organic Fraction of Urban Wastes; Possible Treatments for Energy and/or Material Recovery

The organic fraction of urban wastes is a complex mixture consisting of carbohydrates (mono-, olygo- and polysaccharides), lignin, proteins, fats, and other natural biomolecules. These compounds contain chemical energy which can in principle be recovered and recycled for further use by destructing or destructurating the waste organic molecules.

Indeed, the production of thermal and electric energy exploiting the organic matter of biomasses is one of the current strategies proposed to reduce dependence on fossil fuels [3]. However current technologies have an important critical point consisting in the low conversion of the biomass potential chemical energy. To convert biomass chemical energy to heat and/or electricity, the approaches that can be followed are:

(a) **Incineration**. Energy can be recovered by waste combustion in form of heat, which can be used for generating electricity. However, the high water content of the organic biowastes is a critical factor for their exploitation as fuel. For this reason separately collected organic wastes are commonly not used as feed for incineration facilities or are used in combination with other wastes, or alternatively after bio-drying treatments; but, in this case, the energy sale profits usually do not compensate the overall process costs [4, 5]. Moreover, incineration plants often generate social concern because of the risk of releasing toxic exhaust gases and fine dust particles; in addition the flue gas treatment processes and equipment are very expensive.

(b) **Anaerobic digestion**. During this process part of the organic waste is transformed in biogas by anaerobic microorganisms. The biogas produced is a mixture consisting of methane (44–61 %), CO_2 (25–50 %) and, in lower concentration, steam, H_2S, H_2 and other gases [6]. A schematic representation of the chemical reactions involved in biogas production from organic waste is given in Scheme 1.2.

Although this technology may produce environmental benefits due to the reduction of waste volumes and to the decrease of fossil fuel consumption, its integration in waste treatment plants is limited by the low conversion of the wastes to biogas. For example a typical anaerobic digestion process led to the biodegradation of about 60 % of cellulose and hemicellulose and to a negligible conversion of lignin [8]. No more than 50 % of the starting organic matter is converted to the desired fuel product and fermentation processes lead to organic N mineralization.

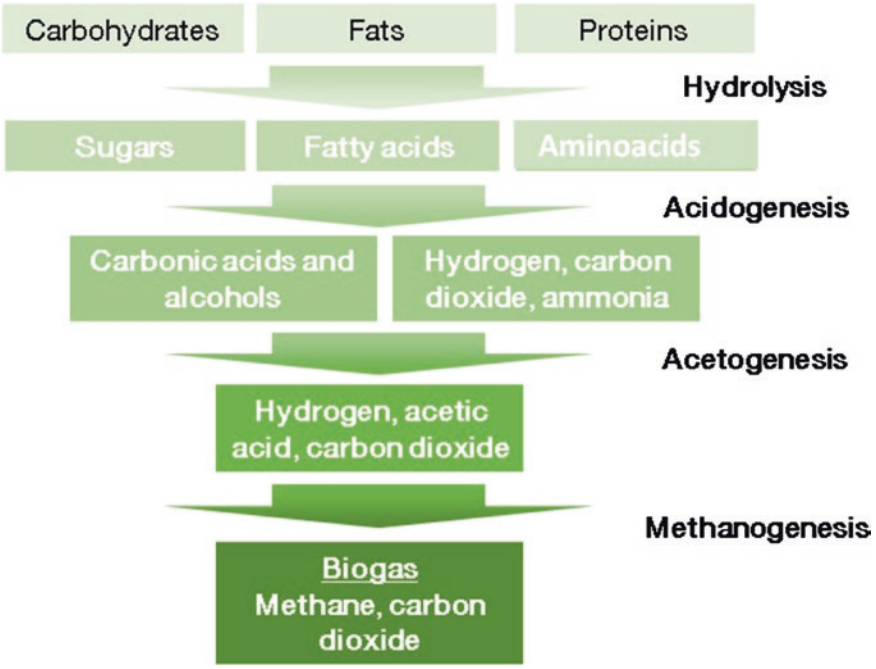

Scheme 1.2 Chemical reactions involved in anaerobic transformation of organic waste to biogas, intermediates and final products [7]

The main reason for the low yield of fermentation processes is that the available microorganisms metabolize mostly the carbohydrate fraction of biomasses, whereas they are not able and/or are inhibited by the lignin fraction [9]. This aspect poses the problem of disposing the residual organic matter for its environmental impact [10]. For this reason the economical final balance for anaerobic digestion is negative and the cost of the obtained fuel is greater than its value. At the present time, the industrial practice in Europe to treat the digestate residue is coupling the anaerobic digestion with the aerobic degradation in order to reach a technical standard product [11].

(c) **Aerobic biodegradation**. In this process bio oxidation is promoted by insufflating air through the waste biomass or by periodically turning the waste pile. During the first days of the treatment, the most biodegradable organics are mineralized giving as a result a stable biomass. The biomass temperature rises up to 70 °C because of the microbial activity, thus in principle allowing the pathogenic microorganisms elimination. Hence aerobic biodegradation could represent an important element of environment protection when processing municipal solid waste. However particular attention has to be paid to control this aspect when aerobic degradation is applied to the treatment of sewage sludge [12].

The aerobic biodegradation can be optimized to evaporate the highest amount of humidity (bio-drying). At aerobic biodegradation treatment times longer than two weeks (maturation), the biomass temperature decreases and weight loss is negligible. Complex reactions take place, involving also lignin, yielding humic acid-like substances. Taking into account the need to comply with precise law requirements, the final matured product of aerobic biodegradation can be sold as compost, a soil conditioner and fertilizer. Obviously, the revenue return for compost sale are strictly related to its quality and to the market demand.

Combustion, anaerobic digestion and aerobic biodegradation allow recovering part of the chemical energy present in the organic residual biomasses, as heat, fuel or fertilizing agent, reducing at the same time the fraction of waste disposed in landfill areas. However, these processes do not produce enough revenue compared to the treatment costs. The greatest cost fraction is compensated by the tipping fees paid to waste treatment companies directly by municipalities, and indirectly by tax payers. Moreover, not all wastes are suitable to be treated by the above techniques, and thus have to be disposed in landfill. Hence, the identification of possible alternative technologies allowing processing different biomass types to produce more remunerative products is desirable. Biofuel production plants could become economically attractive if they were turned into biorefineries by coupling the fuel production process to the treatment of the residual lignocellulosic fraction in order to obtain marketable added value products. This depicts a "step beyond" installations fed with biowaste to produce fuel, energy and chemicals. The present chapter reports results supporting the feasibility of this scenario.

1.2.1 A Real Case of an Integrated Waste Treatment Facility Plant: ACEA Pinerolese

The possibility to exploit urban biowastes (UBW) as source of chemicals to recycle to the chemical industry is rather new [11]. The ultimate trend to optimize the economy and reduce the environmental impact of waste treatment is to build plants integrating the above described approaches. An example of integrated waste treatment processes is the plant operated by ACEA Pinerolese in North West Italy.

The ACEA plant (Fig. 1.1) can be considered a case exemplifying the current state of art in waste management technology. This installation treats biowastes amount to about 50,000 tons year^{-1}, collected from an area of 2,200 km^2 populated by 800,000 inhabitants distributed over 100 municipalities.

ACEA runs an installation designed to optimize energy and material recovery through the concerted operation of different plant sections treating by anaerobic (AN) and/or aerobic (AE) microbial digestion the three main types of UBW, i.e.:

1. the organic humid fraction recovered from town bins deputed to separate source collection of solid urban refuse treated by AE and/or AN,
2. vegetable residues from home gardening and public park trimming treated by AE,
3. the sewage sludge obtained from municipal wastewaters treated by AE.

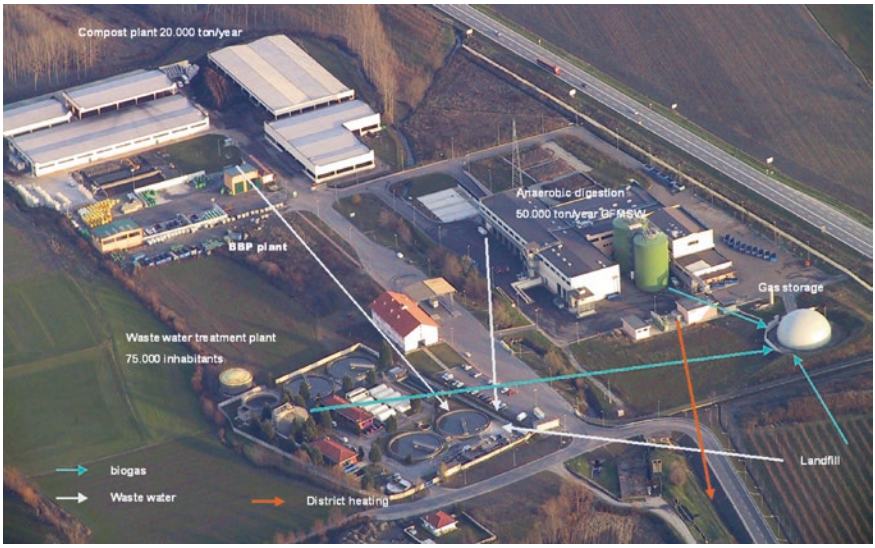

Fig. 1.1 ACEA waste treatment facilities. Notes: *Arrows* indicate energy and material flow among the four compost, AN digestion, wastewater treatment and landfill plant sections

In the plant are present four sections; two for the treatment of solid wastes by AN and AE digestion, the third one for treating wastewaters (WWT) and the last one being a landfill area equipped for biogas collection (LBG). The plant has two safety flares in the AN and LBG sections respectively. The four plant sections are interconnected to maximize biogas and compost yields from biowaste, thus minimizing bio-refuse disposal to landfill. The key technological feature of the plant is the configuration integrating the four AN, AE, WWT and LBG processes. In essence, the bio-organic (humid) fraction of solid urban (FORSU) waste entering the AN process is fermented to yield biogas and a solid digestate (FORSUD) containing residual organic matter not converted to biogas.

The FORSUD material is mixed with green home gardening and park trimmings residues (GR) and/or with sewage sludge (SS) coming from the WWT process. The bio-residues mix is then allowed to undergo fermentation under AE conditions to yield compost.

Compared to the four AN, AE, WWT and LBG processes run in separate plants, the integrated treatment plant allows the achievement of a number of desirable objectives:

- production and/or recovery of renewable bio-fuel from AE and LBG processes
- no FORSUD and less SS disposal to landfill
- less plant surface area needed per treated biowaste ton
- easier odour emission control
- higher recovery of valuable energy and material
- lower environmental impact.

Table 1.1 Examples of biomasses that can be processed and/or produced at the ACEA plant

Biomass	Source
ACEA FORSU T0	Organic humid fraction of urban refuses obtained by separate source collection sampled at the start of the aerobic or anaerobic processing line
ACEA FORSUD	Digestate of the FORSU anaerobic treatment
ACEA CVDF T110	Solid residue recovered after 110 days aerobic digestion of a mix containing FORSUD, green wastes (V) and sewage sludge (F) in the relative weight ratios 35/55/10
ACEA CVU T110	Solid residue recovered after 110 days aerobic digestion of a mix containing FORSU and green wastes (V) mix in the relative weight ratio 33/67
ACSR FOS BIOXT28	Urban refuses fraction 80- sieved, treated for 28 days in cement pool by continuous air insufflation, daily up-side-down turning and water wetting (if necessary) and finally sieved again to
ACSR CVU BIOXT28	Solid residue recovered from 40/60 w/w FORSU/V mix treated as above for 28 days
ACSR CVU T90	Solid residue recovered from 40/60 w/w FORSU/V mix treated as above for 28 days in cement pool and 60 more days in open yard
UB CV T270	Solid residue recovered after 270 days aerobic biodegradation of plant residues
UB CV T360	Solid residue recovered after 360 days aerobic biodegradation of plant residues

Yet, the process economy of the ACEA plant, as well as that of all other waste management plants spread in the world, is not profitable due to operational costs exceeding the market value of the energy and/or materials produced [13, 14].

The plant allows large operational flexibility to produce different types of compost depending on the nature and relative ratios of the bio-residues constituting the AE phase feed. These different out coming biomasses (see Table 1.1) constitute a very interesting starting material to be tested for the isolation of bio-based substances (SBO) and for evidencing possible existing correlation between the physical-chemical properties of the feeding biomass and those of the out coming SBO.

1.3 Isolation of Soluble Bio-based Substances (SBO) from Urban Waste Sourced Biomass

The Department of Chemistry of the University of Torino, within the regional Biochemenergy and national Agrienergia projects, and within the Miseicecrui and the EnvironBOS international projects, has shown that the recalcitrant lignin-like fraction of urban biowastes (UBW) is a cost-effective source of chemical auxiliaries [11] that can find application in diversified fields (Fig. 1.2); e.g. in the formulation of detergents-textile dyeing baths, emulsifiers [15], auxiliaries for soil/water remediation [16] and enhanced oil recovery [17], flocculants, dispersants and binding agents

Fig. 1.2 Schematic representation of the isolation of soluble bio-based substances (SBO) from organic wastes and of the different fields where SBO have been tested

for ceramics manufacture [11], nanostructured materials for chemical [18] and biochemical catalysis [19], plastic materials [20], soil fertilizers and plant biostimulants for agriculture [21, 22] and animal feed supplements [23, 24]. Such variety of applications is possible due to the fact that SBO is a mixture of molecules with molecular weights comprised in a wide range over 5 kD which contain a variety of functional groups (see virtual molecular fragments in Fig. 1.2 and in Sect. 1.4, Fig. 1.4).

Two patent applications for production processes and products have been recently filed [25, 26]. According to the first patent, the MBW streams in the ACEA plant are hydrolyzed in alkaline water to yield a liquid/solid mix which is allowed to settle in order to separate the supernatant liquid hydrolyzate from the insoluble residue (IOR). The recovered liquid phase is circulated through a polysulfone ultrafiltration membrane with 5 kD molecular weight cut-off to yield a retentate with 5–10 % dry matter content. The membrane retentate is dried at 60 °C to yield the final water soluble bio-based product (SBO).

The process is a modified version of the laboratory scale approach where, instead of the hydrolyzed liquid phase ultrafiltration, the acidification of the solution at pH values lower than 1.5 encompasses the precipitation of organic products that show high similarity with humic acid, as described later on.

The upgrade to pilot plant level has been performed thanks to Studio Chiono & Associati in Rivarolo Canavese that made available the space to host the equipment shown in Fig. 1.3.

Fig. 1.3 Pilot plant for SBO isolation. *Inset*: SBO powder and its concentrated water solution

1.4 SBO Characterization

Investigation on the chemical nature of SBO has shown that these substances bear chemical similarities with natural soil and water humic substances (HS). Depending on the sourcing materials, the SBO have been found to be mixtures of molecules differing in molecular weight (MW) from 67 to 463 kg mol^{-1}, and in the content of C-types and functional groups. They are described as likely mixtures of substances formed by long aliphatic carbon chains substituted by aromatic rings and functional groups such as COOH, CON, C=O, PhOH, O-alkyl, O-aryl, OCO, OMe, and NRR′, (R and R′=alkyl or H). These organic moieties derive from fats, proteins, polysaccharides and lignin contained in the sourcing refuse matter which is not completely mineralized by biodegradation. In Table 1.2 compositional data regarding three SBO are reported as an example.

Based on these data a tentative general SBO structure can be hypothesized (Fig. 1.4), evidencing a relevant structural similarities between SBO and natural HS.

Data in Table 1.2 also evidence that a not negligible amount of mineral species is present within SBO composition; however their presence cannot be considered as a drawback since inorganic components can contribute to bring SBO peculiar features, for instance: (i) iron and copper can induce some photoactivity; (ii) Si could be useful as binder in templated synthesis of oxides and/or hybrid materials

Table 1.2 Characterization data of three representatives SBO

(a)

SBO	pH	Volatile solids, w/w %[a]	C, w/w %[a]	N, w/w %[a]	C/N
FORSUD	6.4	84.6	45.07 ± 0.12	7.87 ± 0.12	5.73
CVDFT110	8.2	72.7	35.47 ± 0.09	4.34 ± 0.17	8.17
CVT230	8.2	72.1	38.25 ± 0.09	4.01 ± 0.03	9.54

(b) Mineral elements: Si, Fe, Al, Mg, Ca, K, Na as % w/w[a]; Cu, Ni, Zn, Cr, Pb, Hg as ppm[a]

SBO	FORSUD	CVDFT110	CVT230
Si	0.36 ± 0.03	0.92 ± 0.03	2.55 ± 0.01
Fe	0.16 ± 0.00	0.53 ± 0.02	0.77 ± 0.04
Al	0.78 ± 0.04	0.44 ± 0.02	0.49 ± 0.04
Mg	0.18 ± 0.01	0.49 ± 0.01	1.13 ± 0.06
Ca	1.32 ± 0.05	2.59 ± 0.03	6.07 ± 0.38
K	9.15 ± 0.06	5.49 ± 0.04	3.59 ± 0.21
Na	0.39 ± 0.01	0.15 ± 0.01	0.16 ± 0.01
Cu	100 ± 1	216 ± 1	202 ± 4
Ni	27 ± 1	71 ± 0	92 ± 1
Zn	185 ± 4	353 ± 3	256 ± 1
Cr	11 ± 0	30 ± 1	19 ± 1
Pb	44 ± 2	75 ± 1	85 ± 1
Hg	0.23 ± 0.01	0.45 ± 0.02	0.15 ± 0.02

(c) C types and functional groups[b] concentration as mole fraction of total organic C

SBO	FORSUD	CVDFT110	CVT230
Af	0.43	0.31	0.37
NR	0.10	0.08	0.07
OMe	0.04	0.00	0.00
OR	0.10	0.20	0.14
OCO	0.03	0.07	0.04
Ph	0.10	0.16	0.13
PhOH	0.02	0.06	0.05
PhOY	0.01	0.02	0.02
COOH	0.07	0.09	0.12
CON	0.09	0.01	0.01
C=O	0.01	0.00	0.05
Af/Ar	3.3	1.3	1.8
LH	9.3	5.3	3.6

[a]Concentration values referred to dry matter: averages and standard deviation calculated over triplicates

[b]LH = liphophilic to hydrophilic C ratio; liphophilic C = sum of aliphatic (Af), aromatic (Ph), methoxy (OMe), amide (CON), ammine (NR), alkoxy (RO), phenoxy (PhOY) and anomeric (OCO) C atoms; hydrophilic C = sum of carboxylic acid (COOH), phenol (PhOH) and ketone (C=O) C

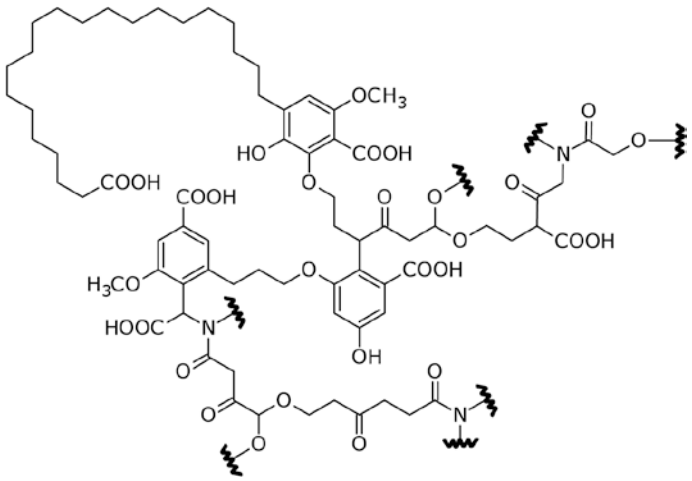

Fig. 1.4 Virtual molecular fragment representing the relative ratios of C types and functional groups. Reproduced with permission of John Wiley and Sons

and (iii) Na and K can act as melting agents. In any case the mineral content does not exceed the values accepted for commercial compost used in agriculture.

Due to the complex chemical composition, the behavior of SBO in water solution cannot be understood as well as for synthetic single molecules. At low concentration, SBO have been found to behave as small surfactant molecules and this aspect can be easily explained taking into account the presence of both hydrophilic and hydrophobic moieties as reported in Table 1.2c. A water surface (γ) tension steep decrease can be observed upon increasing C_{SBO} until a slope change occurs to a more or less flat plateau at 1–2 g L^{-1} C_{SBO} (Fig. 1.5).

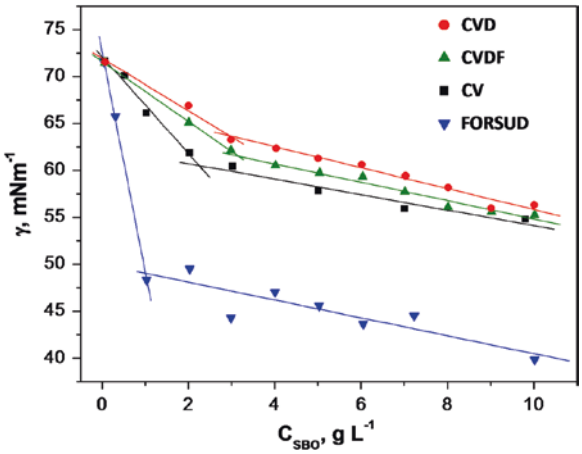

Fig. 1.5 Surface tension (mN m^{-1}) as a function of SBO concentration (g L^{-1}) [15]

Table 1.3 Surfactant data of three representatives SBO

SBO	$-d\gamma_1/dC_{SBO}$[a]	C_1[b] (g L^{-1})	γC_{SBO1}[c] (mN m^{-1})	$-d\gamma_2/dC_{SBO}$[a]
FORSUD	23.3 ± 1.2	0.99	48.85	0.92 ± 0.20
CVDF	3.1 ± 0.8	3.11	61.76	1.0 ± 0.07
CVT230	5.0 ± 0.5	2.10	61.20	0.94 ± 0.12

[a]Slope values for two linear tracts ($d\gamma i/dC_{SBO}$, mN L $m^{-1}g^{-1}$, i = 1, 2)
[b]Concentration (g L^{-1}) at which slope change occurs
[c]Surface tension value at slope change point

The FORSUD seems to lower water surface tension much more than the other two SBO. To appreciate better these differences, each γ–C_{SBO} plot was divided into two tracts which were analyzed by linear regression. Table 1.3 reports the slope values extrapolated from each plot ($d\gamma i/dC_{SBO}$, mN L m^{-1} g^{-1}, i = 1, 2) together with the concentration at which the slope change occurs and the corresponding surface tension value (γ_{CSBO1}). The data allow a more quantitative appreciation of the different behavior of the three investigated SBO. In essence, FORSUD clearly gives the highest $d\gamma_1/dC_{SBO}$ and the lowest C_{SBO1} and γ_{CSBO1} values, whereas CVT230 and CVDF do not seem to exhibit much difference one from the other. Looking at the SBO composition reported in Table 1.2, FORSUD shows the highest liphophilic to hydrophilic C ratio, mostly contributed by aliphatic C.

The SBO surface activity properties correlate with their power to enhance the solubility of hydrophobic compounds in water. At 50–100 g L^{-1} concentration SBO behave more like water soluble polyelectrolytes; they are no longer soluble in water and yield viscous gel-like phases separating from the bulk water phase.

The surfactant properties of SBO play a major role to determine their performance as detergents or auxiliaries for textile dyeing. By virtue of their capacity to lower water surface and interfacial tension they favor the water contact with dirty surfaces. At the same time, they have capacity to form bigger aggregates or to acquire pseudo-micellar conformation in the bulk water phase, and are capable of enhancing the water solubility of hydrophobic materials. Therefore, they can be used to help the transfer of hydrophobic substances from objects to be washed into the water phase. This process has been demonstrated to be effective in washing solutions containing SBO as well as for washing solutions containing synthetic surfactants. This feature opens the possibility to exploit SBO aqueous solutions also for the remediation of soils contaminated by organics, through the so-called soil washing approach.

The surfactant behavior of SBO can be also exploited in dyeing textiles. In this case, SBO have been shown to be capable of binding water soluble or insoluble dyes, and modulate their transfer kinetics to the surface of the fabric to be dyed, thus yielding fabrics dyed as intensely and homogeneously as synthetic surfactants [11].

The capacity of the SBO molecules to acquire different conformation and/or yield large macromolecular aggregates in solution has offered scope to investigate these substances as templates for the synthesis of nanostructured materials.

Also, their structural similarity with HS, and the properties of HS as photosensitizers and their role in soil fertility, has stimulated investigation of SBO for specific applications in environmental remediation and agriculture. Details for specific applications are reported in the above cited papers.

1.5 New Processes and Products Under Investigation

SBO obtained at laboratory scale were isolated in their acidic form; on the contrary, when the isolation process was implemented at pilot-plant scale, the acidification step was substituted with an ultrafiltration step, exploiting the different size of "humic like" and "fulvic like" components of SBO. In such a way, SBO have been obtained as potassium salts, easier to be dissolved in water prior to their use. Despite the two processes should yield products differing only for their acidic or salt form, the pilot-plant derived SBO showed a peculiar behavior at pH lower than 1.5. Indeed, at this pH, about 10 % in weight of SBO stayed in solution, whereas 90 % precipitated. The fraction of SBO (hereinafter SBO_{sol}) soluble at pH < 1.5 showed peculiar properties as reported below.

The SBO_{sol} deserved our attention because it was not previously characterized despite preliminary not published results indicate a stronger photosensitizing effect compared to SBO itself. Particular attention was devoted to the presence and evolution, upon irradiation with simulated solar light, of acidic functions, that can in principle participate in iron ions coordination. Indeed, among many possible application of SBO as photosensitizer in Advanced Oxidation Technologies [27], SBO have been recognized as promising compounds to perform photo-Fenton process at mild condition, because of their capability to maintain Fe(III) in solution without lowering the pH below value about 4.5–5 [28].

Here we show the results of a potentiometric study devoted to identify and quantify acidic functions before and after irradiation of SBO_{sol} with simulated solar light. pH-metric titrations were performed on $CVT230_{sol}$ and on $CVDF_{sol}$ derived from the treatment of 500 mg L^{-1} solutions irradiated with simulated solar light for 15 h. The titrant was KOH 0.1 mol L^{-1}, the temperature was maintained at 25 ± 0.1 °C and the ionic strength was 0.1 mol L^{-1} (medium: tetraethylammonium chloride). The titration curves obtained were compared with the curves attained with not irradiated $CVT230_{sol}$ and $CVDF_{sol}$. It was found that the irradiation process leads to increase of the acidity of the SBO solutions. This phenomenon was observed for both $CVT230_{sol}$ and $CVDF_{sol}$ products, but is less marked for $CVDF_{sol}$. The experimental curves were elaborated in order to attain a chemical model of the SBO aggregates suitable to explain their acid-base behavior. With the software BSTAC [29] it was possible to calculate the concentration of protogenic sites and the relative protonation constants (Table 1.4). The literature dealing with protonation of HS assumes that the total concentrations of COOH and PhOH functional groups can be obtained as the sum of the concentration values for the species with log K_a < 8 for COOH and with logK_a > 8 for PhOH [30]. In this

Table 1.4 Chemical models, protonation constants and concentration of protogenic sites obtained from the elaboration of titration data

SBO	Protogenic site	log β^a	Conc. (mmol g^{-1})[e]
$CVT230_{sol}$	Hcvt1	3.1 ± 0.1	0.91
	Hcvt2	6.0 ± 0.2	0.41
	Hcvt3	9.66 ± 0.06	0.93
	Weighted standard deviation of the fit	3.20	
$CVT230_{sol}$ irradiated	Hcvt1	1.96 ± 0.5	5.00
	Hcvt2	5.3 ± 0.2	0.39
	Hcvt3	9.53 ± 0.06	0.97
	Weighted standard deviation of the fit	3.34	
$CVDF_{sol}$	Hcvdf1	2.4 ± 0.3	1.94
	Hcvdf2	4.7 ± 0.1	0.64
	Hcvdf3	7.6 ± 0.2	0.41
	Hcvdf4	9.8 ± 0.1	0.77
	Weighted standard deviation of the fit	2.88	
$CVDF_{sol}$ irradiated	Hcvdf1	2.7 ± 0.2	1.73
	Hcvdf2	4.6 ± 0.1	0.77
	Hcvdf3	7.1 ± 0.2	0.45
	Hcvdf4	9.7 ± 0.1	0.98
	Weighted standard deviation of the fit	2.38	

[a]The protonation constants are expressed as log of $\beta_r = [AH_r^{-n+r}]/[A^{-n}][H^+]^r$
[b]Different numbers refer to different acidic monoprotic sites
[c]±Standard deviation
[d]Weight for each experimental point is given as $w = 1/s^2$ [29]
[e]The concentration of the protogenic sites are expressed with respect to the mass of the SBO used to prepare the solution

case, the attribution of log K values to a specific functional group is not allowed because, as shown in Table 1.2, all SBO present also amines or other nitrogen functions. However, it is reasonable to suppose that the log $K_a < 7$ can be attributed to –COOH groups. The total concentration of –COOH, calculated as the sum of the concentrations of the species with a log $K_a < 7$ obtained from the chemical model, results affected by the irradiation process only for $CVT230_{sol}$. In this case, the –COOH mmol g^{-1} concentrations are 1.3 ± 0.2 and 5.4 ± 0.2 for the $CVT230_{sol}$ and $CVT230_{sol}$ after irradiation, respectively. As for $CVDF_{sol}$, the irradiation process seems affect only the concentration of the less acidic species.

Based on these data it can be hypothesized that irradiation would not negatively influence the capability of the SBO_{sol} to promote Fenton like processes; nevertheless, further investigation is needed at this purpose.

References

1. UNESCAP Green Growth Path. (2014). www.greengrowth.org. Last access June, 2014.
2. European directives: 91/156/CEE, 91/689/CEE, 94/62/CE.

3. Kaminsky, J. (2004). Development of strategies for deployment of biomass resources in the production of biomass power. NREL/SR-510-33524, available electronically at http://www.nrel.gov/docs/fy04osti/33524.pdf.
4. Montoneri, E., Savarino, P., Bottigliengo, S., Boffa, V., Bianco Prevot, A., Fabbri, D., & Pramauro, E. (2009). Biomass wastes as renewable source of energy and chemicals for the industry with friendly environmental impact. *Fresenius Environmental Bulletin, 18*, 219–223.
5. Fantozzi, F., & Buratti, C. (2009). Biogas production from different substrates in an experimental continuously stirred tank reactor anaerobic digester. *Bioresource Technology, 100*, 5783–5789.
6. Tambone, F., Genevini, P., D'Imporzano, G., & Adani, F. (2009). Assessing amendment properties of digestate by studying the organic matter composition and the degree of biological stability during the anaerobic digestion of the organic fraction of MSW. *Bioresource Technology, 100*, 3140–3142.
7. www.clarke-energy.com/gas-type/biogas/. Last access July 2014.
8. Kraft, E., Bidlingmaier, W., De Bertoldi, M., Diaz, L. F., & Barth, J. (2006). Biological waste management from local to global. In *Proceedings of the International Conference ORBIT 2006, Weimar* (pp. 1201–1210), ISBN 3-935974-09-4.
9. Mabee, W. E., Gregg, D. J., Arato, C., Berlin, A., Bura, R., Gilkes, N., et al. (2006). Updates on softwood-to-ethanol process development. *Applied Biochemistry and Biotechnology, 129*, 55–70.
10. Lusk, P. (1998). Methane recovery from animal manures. The current opportunities casebook. NREL/SR-580-25145, available electronically at http://www.nrel.gov/docs/fy99osti/25145.pdf.
11. Montoneri, E., Mainero, D., Boffa, V., Perrone, D. G., & Montoneri, C. (2011). Biochemenergy: a project to turn an urban wastes treatment plant into biorefinery for the production of energy, chemicals and consumer's products with friendly environmental impact. *International Journal of Global Environmental Issues, 11*, 170–196.
12. EPA/625/R-92/013, available electronically at www2.epa.gov/sites/production/files/documents/625R92013ALL.EPA/625/R-92/013.
13. Rathi, S. (2007). Optimization model for integrated municipal solid waste management in Mumbai, India. *Environment and Development Economics, 12*, 105–121. doi:10.1017/S1355770X0600341X, available at www.environmental-expert.com/Files%5C5253%5Carticles%5C14338%5Cart6.pdf.
14. Bech, R. W. (2004). Anaerobic Digestion Feasibility Study, Final report for the Bluestem Solid Waste Agency and Iowa Department of Natural Resources, available at www.iowadnr.gov/waste/policy/files/bluestem.pdf.
15. Vargas, A. K. N., Bianco Prevot, A., Montoneri, E., Le Roux, G. C., Savarino, P., Cavalli, R., et al. (2014). Use of biowaste-derived biosurfactants in production of emulsions for industrial use. *Industrial and Engineering Chemistry Research, 53*, 8621–8629.
16. Montoneri, E., Tomasso, L., Colajanni, N., Zelano, I., Alberi, F., Cossa, G., & Barberis, R. (2014). Urban wastes to remediate industrial sites: A case of polycyclic aromatic hydrocarbons contamination and a new process. *International Journal of Environmental Science and Technology, 11*, 251–262.
17. Baxter, M. D., Acosta, E., Montoneri, E., & Tabasso, S. (2014). Waste biomass-extracted surfactants for heavy oil removal. *Industrial and Engineering Chemistry Research, 53*, 3612–3621.
18. Boffa, V., Perrone, D. G., Magnacca, G., & Montoneri, E. (2014). Role of a waste-derived biosurfactant in the sol-gel synthesis of nanocrystalline titanium dioxide. *Ceramic International, 40*, 12161–12169.
19. Magnacca, G., Laurenti, E., Vigna, E., Franzoso, F., Tomasso, L., Montoneri, E., & Boffa, V. (2012). Refuse derived bio-organics and immobilized soybean peroxidase for green chemical technology. *Process Biochemistry, 47*, 2025–2031.
20. Franzoso, F., Tabasso, S., Antonioli, D., Montoneri, E., Persico, P., Laus, M., Mendichi, R., & Negre, M. (2014). Films made from poly (vinyl alcohol-co-ethylene) and soluble biopolymers isolated from municipal biowaste. *Journal of Applied Polymer Science*. doi:10.1002/app.41359.

21. Sortino, O., Montoneri, E., Patanè, C., Rosato, R., Tabasso, S., & Ginepro, M. (2014). Benefits for agriculture and the environment from urban waste. *Science of the Total Environment, 487C*, 443–451.
22. Baglieri, A., Cadili, V., Mozzetti Monterumici, C., Gennari, M., Tabasso, S., Montoneri, E., et al. (2014). Fertilization of bean plants with tomato plants hydrolysates. Effect on biomass production, chlorophyll content and N assimilation. *Scientia Horticulturae, 176*, 194–199.
23. Montoneri, C., Montoneri, E., Tomasso, L., & Piva, A. (2013). Compost derived substances decrease feed protein N mineralization in swine cecal fermentation. *Journal of Agricultural Science, 13*, 31–44.
24. Dinuccio, E., Biagini, D., Rosato, R., Balsari, P., Lazzaroni, C., & Montoneri, E. (2013). Use of acid soluble bio-organic substances extract as rabbits feed additive to reduce manure gases emission during storage. *Advances in Animal Biosciences, 4*(Special Issue 2), 515–520.
25. Montoneri, E., & Montoneri, C. (2012). Biopolymers isolated from residual biomass and fossil source; production processes and product uses. International Patent Application by the University of Torino, 21.12.2012, NO. PCT/IT2012/000399.
26. Montoneri, E. (2013). Plastic materials containing products isolated from residual biomass and fossils, and their sulfonated derivatives. International patent application by Acea Pinerolese, 06.12.2013, NO. PCT/IT2013/000339.
27. Avetta, P., Bella, F., Bianco Prevot, A., Laurenti, E., Montoneri, E., Arques, A., & Carlos, L. (2013). Waste Cleaning Waste: photodegradation of monochlorophenols in the presence of waste-derived photosensitizer. *ACS Sustainable Chem Eng, 1*, 1545–1550.
28. Gomis, J., Carlos, L., Bianco Prevot, A., Teixeira, A. C. S. C., Mora, M., Amat, A. M., Vicente, R., & Arques, A. (2014). Bio-based substances from urban waste as auxiliaries for solar photo-Fenton treatment under mild conditions: Optimization of operational variables. Catal Today, available online http://dx.doi.org/10.1016/j.cattod.2014.03.034.
29. De Stefano, C., Mineo, P., Rigano, C., & Sammartano, S. (1993). Ionic-strength dependence of formation-constants. The calculation of equilibrium concentrations and formation-constants. *Annales de Chimie, 83*, 243–277.
30. Santos, E. B. H., Esteves, V. I., Rodrigues, J. P. C., & Duarte, A. C. (1999). Humic substances' proton-binding equilibria: Assessment of errors and limitations of potentiometric data. *Analytica Chimica Acta, 392*, 333–341.

Chapter 2
Photogeneration of Reactive Oxygen Species by SBO and Application in Waste-Water Treatment

Luciano Carlos and Daniel O. Mártire

Abstract Soluble bio-based substances (SBO) extracted from urban bio-wastes have similar chemical properties to humic substances (HS) present in natural waters and soils. Therefore, SBO are also expected to have photochemical properties similar to HS. In this chapter, a summary of the photochemistry of HS is presented along with the recent advances related to the photogeneration of reactive species upon irradiation of aqueous solutions of SBO and some examples of pollutant degradation photo-induced by SBO.

Keywords Soluble bio-based substances (SBO) · Humic substances · Reactive oxygen species (ROS) · Wastewater · Emerging pollutants · Solar processes · Photo-Fenton

2.1 Introduction

Recently, urban bio-wastes have been shown as a potential cost-effective renewable source of soluble bio-based substances (SBO) [1]. The organic fraction of these materials has similar chemical nature and properties to humic substances (HS) present in natural waters and soils [2–4]. Therefore, SBO is expected to have photochemical properties similar to HS, which represent the main fraction of chromophoric dissolved organic matter (CDOM) that absorbs solar radiation. For this reason, a summary of the photochemically mediated processes induced by HS is outlined below.

L. Carlos (✉)
Instituto de Investigación y Desarrollo en Ingeniería de Procesos, Biotecnología y Energías Alternativas, PROBIEN (CONICET-UNCo), Buenos Aires, 1400, Neuquén, Argentina
e-mail: luciano.carlos@probien.gob.ar

D.O. Mártire
Instituto de Investigaciones Fisicoquímicas Teóricas y Aplicadas (INIFTA), CCT-La Plata-CONICET, Universidad Nacional de La Plata, Diag, 113 y 64, La Plata, Argentina
e-mail: dmartire@inifta.unlp.edu.ar

A. Arques and A. Bianco Prevot (eds.), *Soluble Bio-based Substances Isolated From Urban Wastes*, SpringerBriefs in Green Chemistry for Sustainability,
DOI 10.1007/978-3-319-14744-4_2

2.2 Photochemistry of HS

The UV-vis absorption spectra of Pahokee Peak humic acid (Fig. 2.1) decreases exponentially with increasing wavelength [5, 6], providing to aquatic organisms protection from damaging UV radiation, and giving color to surface waters. Spectra are often fit to Eq. 2.1, where $a(\lambda)$ is the absorption coefficient at wavelength λ, $a(\lambda_0)$ is the absorption coefficient at a reference wavelength, and S is the spectral slope parameter [7].

$$a(\lambda) = a(\lambda_o) \times e^{-S(\lambda-\lambda_0)} \tag{2.1}$$

Higher values of S indicate a more rapid decline and a lower absorption contribution in the visible wavelengths. The ratio at two different wavelengths, e.g. 465 and 665 nm (namely E4/E6 ratio) was also employed to characterize the spectra [8]. The increase of molecular complexity of HS by formation of more extended and oxidized aromatic systems is expected to decrease the E4/E6 due to the relative increment of the absorption coefficient in the red region of the visible spectrum [9].

Recently, a model of the optical properties of HS was proposed [10]. In this model the absorption and emission spectra of HS arise from a very large number of absorbing and emitting states, where intramolecular electronic interactions between donor–acceptor chromophores play an important role. These electronic interactions between chromophores produce an array of photophysical and photochemical reaction channels. The relative importance of each channel varies with the HS source and environmental conditions due to varying abundance of electron donating and accepting groups and the effects of solution chemistry on excited-state energies [11].

The absorption of light by aqueous HS leads to the formation of several reactive species, as shown in Scheme 2.1.

The excited singlet states of HS (^{1}HS*) populated upon light absorption process (reaction 1) decay by: (i) fluorescence and internal conversion to ground state

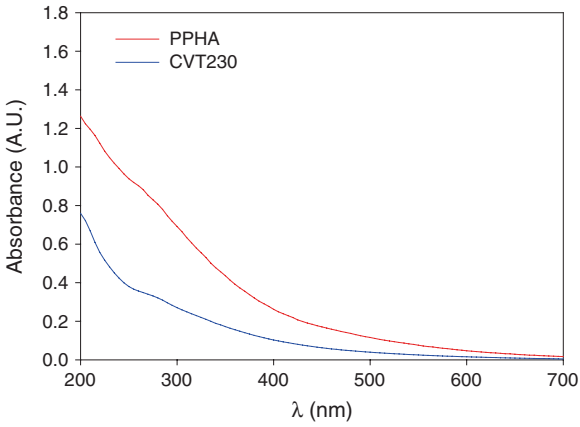

Fig. 2.1 UV-vis absorption spectra of Pahokee peat humic acid (20 mg L^{-1}) and SBO, namely CVT230 (20 mg L^{-1}) in water at pH 7.0

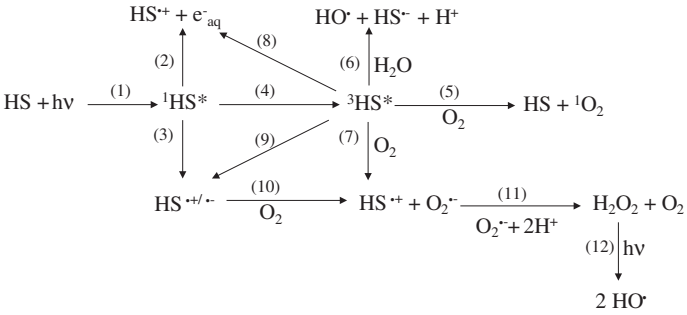

Scheme 2.1 Photogeneration of reactive species

(pathways not shown in Scheme 2.1), (ii) to yield radical cations ($HS^{\cdot+}$) and solvated electrons e^-(aq.) (photoionization process 2), (iii) to charge-separated species ($HS^{\cdot+/\cdot-}$) formed by donor–acceptor electron transfer (reaction 3) or (iv) through intersystem crossing to the excited triplet states ($^3HS^*$) (reaction 4).

Photoionization of aromatic groups of HS at excitation wavelengths from 250 to 400 nm leads to the formation of hydrated electrons e^-(aq.) [12, 13]. The quantum yields of e^-(aq.) generation is about 10^{-5} to 10^{-4} over the wavelength range from 300 to 400 nm [12, 14].

Triplet quantum yields are estimated to lie between 0.01 and 0.1 [15]. Reported values of the energy of the excited triplet states of HS ($^3HS^*$) are over the range 180–250 kJ mol^{-1} [16, 17]. Production of $^1O_2$ by HS occurs via energy transfer from $^3HS^*$ to ground-state O_2 (reaction 5). Other decay routes of $^3HS^*$ involve electron transfer processes (reactions 6–9).

The quantum yield of $^1O_2$ formation lies in the range of 0.01–0.1, increases with decreasing excitation wavelength in the visible and near-UV and depends on the HS source and solution pH [18, 19].

Photogeneration of $O_2^{\cdot-}$ is mainly related to the population of charge-transfer states ($HS^{\cdot+/\cdot-}$) from $^1HS^*$ and $^3HS^*$ (reactions 3 and 9) of HS and subsequent reduction of oxygen to O_2 (reaction 10) [19]. Hydrogen peroxide is produced by dismutation of $O_2^{\cdot-}$ (reaction 11) [20]. Quantum yields for H_2O_2 production are also wavelength-dependent and at ca. 350 nm range from 5×10^{-5} to 10^{-3} for different samples [11].

The photogeneration of hydroxyl radical ($HO^{\cdot}$), a highly reactive oxidant that unselectively reacts at near diffusion-controlled rates with most organic substrates, was widely investigated [21–23]. Although there is evidence for the involvement of oxygen-dependent, oxygen-independent and hydrogen peroxide-dependent pathways, the mechanism still remains unclear [21, 22]. Possible generation pathways include the photolysis of hydrogen peroxide (reaction 12) and hydrogen abstraction from water by the excited triplet state of substituted benzoquinones, which are components of HS (reaction 6). In the presence of iron, $HO^{\cdot}$ can also be formed through Fenton-like chemistry involving H_2O_2 and a HS photo-reductant [21, 24].

The UV-visible absorption of HS is very sensitive to changes produced by photolysis [25]. Bosio et al. [26] investigated the changes in the absorption spectra of 0.1 g L^{-1} solution of Aldrich Humic Acid upon irradiation with excitation wavelengths $\lambda > 320$ nm. From changes in the UV-visible spectra taken at different irradiation times and under various conditions it was possible to elucidate the involvement of the photogenerated reactive oxygen species (ROS) in the photodegradation of the humic acid. The observed changes increase with increasing oxygen concentration in the solutions, in line with ROS involvement in the photodegradation process. Experiments carried out with specific chemical probes showed that the participation of $^1O_2$ and $HO^{\cdot}$ in the photodegradation of HS seems to be more relevant than that of $O_2^{\cdot-}$. The effect of H_2O_2 was found to be negligible.

2.3 Photochemical Generation of ROS by SBO

Generation of ROS upon irradiation of HS solutions was discussed in the previous section. Because of the similar estimated molecular weights and the pH-dependence of their solubility, SBO should be compared to humic rather than to fulvic acids. The generation of ROS upon irradiation of two types of SBO, namely AC8 and CVT230, has been investigated with the purpose of employing these substances as photosensitizers in the degradation of organic contaminants present in waste waters. To this aim in situ electronic paramagnetic resonance (EPR) experiments using the spin trapping approach were performed [27, 28]. This method involves the addition of transient radical species to a diamagnetic compound (spin trap), with the formation of a paramagnetic persistent radical (spin-adduct). In general, the spin-adduct is more stable than the original free radical and can be analyzed afterwards with EPR spectroscopy. The spin trap, generally a nitrone or nitroso compound, must be stable under the reaction conditions, undergo radical addition quickly in order to avoid further reactions of the radicals before the trapping, and not suffer secondary. The compounds 4-oxo-TMP (45 mM) and DMPO (17.4 mM) were employed as trapping agents for $^1O_2$ and $HO^{\cdot}$, respectively [29].

Irradiation experiments in the presence of various amount of SBO (concentration $\leq$2 g L^{-1}) showed that the intensity of 4-oxo-TEMPO is proportional to AC8 concentration. Similar experiments performed with CVT230 in the concentration range up to 5 g L^{-1} showed the same trend. However, the concentration of the DMPO-OH adduct increases as SBO (either AC8 or CVT230) concentration increases until a maximum value of about 20–50 mg L^{-1}, and then decreases at higher concentration of SBO. This behavior can be explained considering the competition between production and scavenging of $HO^{\cdot}$ radicals. This result is in line with reported changes in the UV-visible spectrum of SBO upon irradiation (see next section).

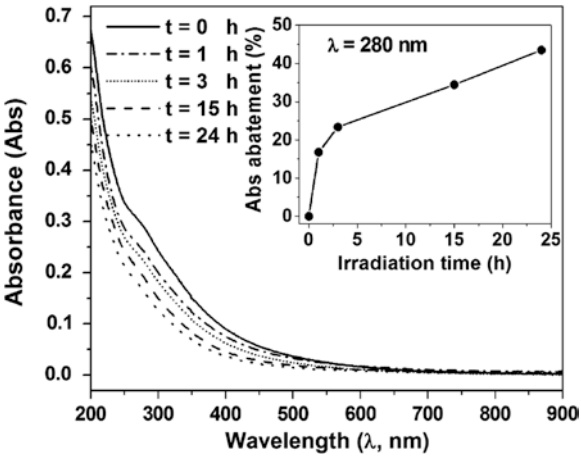

Fig. 2.2 UV-vis spectra of 150 mg L^{-1} AC8 aqueous solution at variable irradiation times, recorded after 10× sample dilution. Inset: absorbance (Abs) abatement % at 280 nm versus irradiation time. From Ref. [30]. Reproduced with permission of Elsevier

2.4 Photostability of SBO

The photostability of SBO in aqueous solution under steady-state irradiation was followed by measuring its UV-visible spectrum concentration at different irradiation times. Figure 2.2 shows the decrease in the UV-VIS absorbance of a 150 mg L^{-1} AC8 solution upon irradiation ($\lambda > 340$ nm). The inset of Fig. 2.2 shows the evolution of the absorbance at 280 nm. Several functional groups could be responsible for the absorption around 280–300 nm, which arises from π to π^* electron transitions occurring in phenolic arenes, benzoic acids, aniline derivatives, polyenes and polycyclic aromatic hydrocarbons with two or more rings [30]. Moreover, the presence of aromatic moieties as major molecular components of AC8 was confirmed by ^{13}C NMR spectroscopy [29]. Since irradiation was performed with $\lambda > 340$ nm, direct photolysis of chromophores absorbing at 280 nm should be neglected. Thus, the AC8 photodegradation should arise from population of excited states of other chromophores, which promote the formation of reactive species able to react with aromatic moieties. As a result, the absorbance of SBO at 280 nm decreases.

2.5 Application of SBO for the Photo-Degradation of Pollutants in Waters

Based on the photochemical properties of SBO and their capacity of generating reactive species, the application of these substances as photosensitizers in wastewater treatment could constitute a very convenient and sustainable alternative to the conventional treatments from both the economic and ecological point of view. Moreover, the use of SBO for water detoxification may be considered a green

process since it valorizes solid waste as a material of technological application. Taking this into account, many studies were encouraged to elucidate the potential applications of SBO employing UVB-UVA, simulated solar light and real solar light as irradiation sources to degrade different kind of pollutants, such as dyes, naphthalene sulfonates, chlorophenols, and emerging pollutants.

In this section, we have compiled different investigations of the degradation of the pollutants specified above photo-induced by SBO.

2.5.1 Dye Degradation

Three commercial sulfonated azo-dyes, ethylorange (EO), Orange I (OI) and Orange II (OII) were photo-degradated under simulated solar irradiation in the presence of SBO isolated from urban yard trimmings (cHAL3) and from a 1:1 (w/w) mix of food (humid) and green residues at the start of the aerobic digestion process (cHAL6) [31]. Aqueous solutions of these azo-dyes at 5 mg L^{-1} concentration have been irradiated in the presence of variable amounts of cHAL3 and cHAL6. Figure 2.3 shows that an increase in the SBO/EO ratio, yields higher dye % abatement. In particular a complete removal of EO can be achieved with cHAL6, indicating that SBO can be successfully used as photosensitizers. Also, the results demonstrate that in all cases nearly quantitative dyes abatement can be achieved with kinetics following a pseudo first-order law. On the other hand, the comparison of dye abatement rate, solution bleaching and sulfate evolution (as indicator of the dye mineralization) showed that the photobleaching is delayed compared to the dye disappearance and the amount of sulfate is lower than the stoichiometric value. These results can be associated with the formation and accumulation of colored intermediates containing the sulfonic group.

The photodegradation of aqueous solutions of the cationic xanthenic dye crystal violet (CV) was also studied. In this case, photochemical experiments were carried

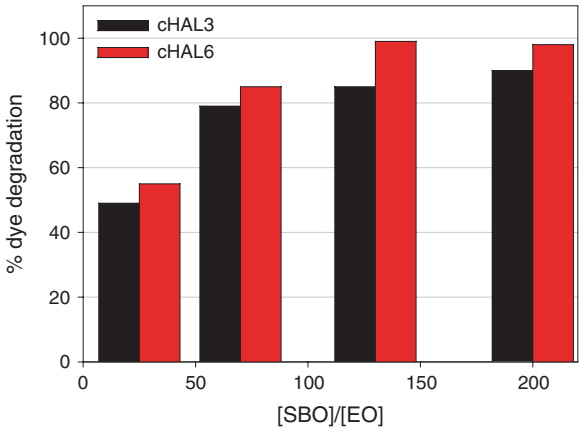

Fig. 2.3 Dye % degradation versus cHALi (i = 3 or 6)/EO (w/w) ratio after 3 h irradiation in Solarbox

Table 2.1 Apparent bleaching constant (k_{app}) as a function of SBO content

SBO (mg L^{-1})	k_{app} ($\times 10^3$ min^{-1})
–	0.60 ± 0.05
2.5	1.30 ± 0.06
5	3.10 ± 0.19
10	3.20 ± 0.08
25	3.70 ± 0.13
50	2.84 ± 0.14
100	2.19 ± 0.06
200	1.68 ± 0.04

out in a reactor equipped with a medium-pressure mercury arc lamp with a glass jacket to cut-off the radiation with wavelengths shorter than 300 nm and with the specific SBO, referred to as CVT230, isolated from the alkaline hydrolyzate of urban private gardening and public park trimming residue compost. The role of CVT230 on the photobleaching of CV in aqueous solution was investigated by recording the absorption spectra of CV at different irradiation times. A noticeable decrease of the CV absorbance at 532 nm was observed. The discoloration kinetics was fitted to a pseudo-first order law and an apparent bleaching constant (k_{app}) for each experimental condition was calculated. The irradiation of CV solutions performed in the absence and presence of different amounts of CVT230 clearly shows that SBO promote the indirect photochemical degradation of CV (Table 2.1). The results show that SBO enhance the photobleaching of CV solutions with an optimal SBO concentration of ca. 20 mg L^{-1}. Mechanistic investigation based on chemical probes and changes in the absorption spectrum of CV in the presence of SBO seems to indicate that a complex formed between sensitizer and substrate plays a major role in the process [32].

2.5.2 Naphthalene Sulfonates Degradation

Naphthalene sulfonates are widely employed in many industrial processes as dispersants, stabilizers, suspending and wetting agents, and intermediates for dye synthesis. In this section, the removal efficiency of naphthalene sulfonates photoinduced by SBO is discussed. Four different naphthalene sulfonates, 1-naphthalenesulfonic sodium salt (1-NS), 2-naphthalenesulfonic sodium salt (2-NS), 1,5-naphthalenedisulfonic acid (1,5-NdS) and 2,6-naphthalenedisulfonic disodium salt (2,6-NdS), have been used as substrates. The SBO used in this study, referred to as AC8, was sourced from a UBW that was the product of the aerobic digestion of a 2:1 food/green residue mixture aged for 110 days. The results showed that 4 h irradiation of solutions containing 20 mg L^{-1} of the probe substrates in the presence of 50–500 mg L^{-1} AC8 increases the degradation yield to 15–30 %. Also, substrate and sulfate ion concentration were monitored at different irradiation times. The results obtained for experiments with 150 mg L^{-1} AC8 are shown in

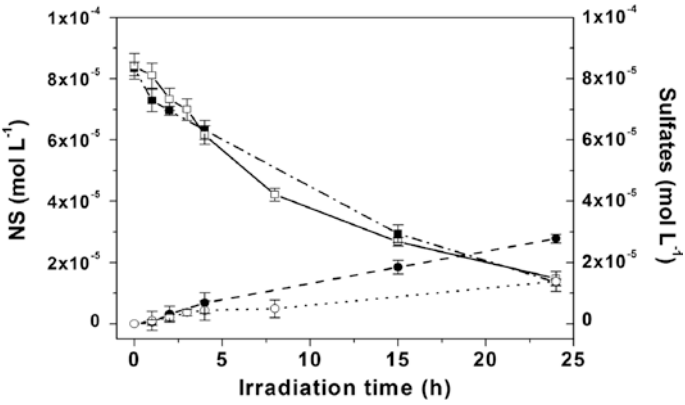

Fig. 2.4 Concentrations of naphthalene sulfonates (NS) and sulfates (mol L^{-1}) versus irradiation time (h) in the presence of 150 mg L^{-1} AC8: data for 1-NS (*filled square*) and 2-NS (*open square*) substrates and for the sulfates released from 1-NS (*filled circle*) or 2-NS (*open circle*) degradation. From Ref. [30]. Reproduced with permission of Elsevier

Fig. 2.4. The data, based on substrate depletion, indicate that after 24 h irradiation, 65–80 % of substrate removal is obtained. In the presence of AC8, photodegradation of the sulfonates seems to be slightly faster than that of the disulfonates. This lesser reactivity of the latter might result from the lower electron density of the aromatic nuclei and, thus, reduced electron availability for the electrophilic ROS.

Among several possible ROS species formed upon AC8 irradiation, previous work has provided evidence for the formation of $HO^{\cdot}$ radicals and singlet oxygen [29] (see Sect. 2.3). Irradiation experiments of 2-NS and 1,5-DNS in the presence of 2-propanol (0.01 M), an $HO^{\cdot}$ radical scavenger [33], showed a significant decrease in the percentage degradation for both substrates. These results confirm the relevant role played by the $HO^{\cdot}$ radicals in the photodegradation process [30].

2.5.3 Chlorophenols Degradation

2-chlorophenol (2-CP), 3-chlorophenol (3-CP) and 4-chlorophenol (4-CP) were chosen as target substrates because of their environmental relevance. They belong to a class of priority toxic pollutants listed by the US EPA; they are toxic, hardly biodegradable and their removal from the environment is complex.

Photochemical experiments using a solarbox as irradiation source and in the presence of CVT230 as SBO source were conducted. Aqueous solutions of each chlorophenol (1×10^{-4} M) were irradiated in the presence of CVT230 (500 mg L^{-1}), at an initial pH = 9.4, value obtained by simply dissolving SBO in water at the indicated concentration. A progressive degradation for all the substrates up to their complete disappearance within 24 h of irradiation is obtained

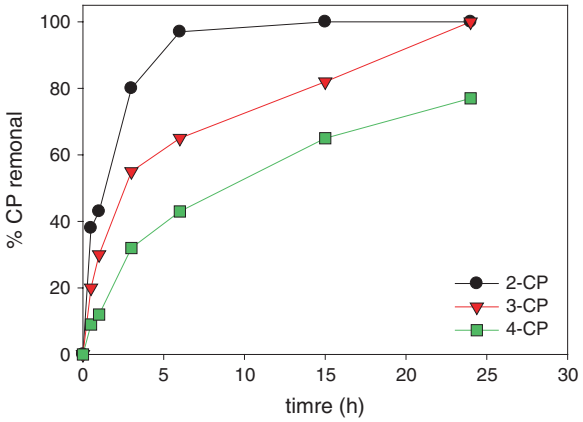

Fig. 2.5 Percentage of substrate degradation in the function of the irradiation time. [chlorophenols]$_0 = 1.0 \times 10^{-4}$ M; [CVT230]$_0 = 500$ mg L^{-1}

(Fig. 2.5). Substrate degradation curves can be fitted to a pseudo-first order degradation law. The reactivity order observed for the three substrates was 2-CP > 3-CP > 4-CP. On the other hand, the monitoring of chloride ion in this experiment, revealed that a close relationship between the degradation of each chlorophenol and the chloride ion formation [34]. After 24 h, the mineralization of organic Cl is 70 % for 4-CP and nearly quantitative for 2-CP and 3-CP. These results suggest that dechlorination occurs at the early stages of the reaction, and formation of major amounts of chlorinated organic byproducts should not be expected.

The pH showed to play a significant role in the degradation of chlorophenols. Lower degradation rates were obtained in experiments performed at neutral pH. This result can be discussed taking into account the acid/base properties of chlorophenols (pKa values around 9–10). The bimolecular rate constants for the reactions of singlet oxygen with the basic forms of chlorophenols are two orders of magnitude higher than those corresponding to the acidic forms [35]. Instead, the reactions of HO radical with chlorophenols are not significantly affected by the dissociation of the substrates. This suggests that singlet oxygen might play a major role in the photooxidation of chlorophenols under the studied experimental conditions.

2.5.4 Emerging Pollutants Degradation

A solution containing a mixture of the six emerging pollutants (EP), namely acetaminophen, caffeine, amoxicillin, carbamazepine, acetamiprid and clofibric acid (5 mg L^{-1} of each EP) was used as probe in the photochemical experiment.

A solar simulator as irradiation source and different amounts of CVT230 (20 and 200 mg L^{-1}) were used. It is important to mention that almost all the EPs were significantly degraded in the absence of CVT230 by direct photolysis (except for carbamazepine and caffeine which present low quantum efficiencies of consume) [36]. The presence of the CVT230 in the experiments resulted in a significant decrease in the photolysis rate of the pollutants, as shown by the calculated pseudo-first order rate constants of each EP which were reduced up to 50 % in the presence of 20 mg L^{-1} of CVT230 and even 80 % with 200 mg L^{-1}. This behavior can be attributed to a light screening effect of the highly colored organics CVT230 over the direct photolysis of each EP. Despite these results, CVT230-mediated photogeneration of reactive species that contribute to the indirect photolysis of the EP should not be ruled out [37].

The addition of H_2O_2 to the reaction medium at pH 7 resulted in a faster photodegradation of the EPs in the absence of CVT230 for almost all the EPs (except for clofibric acid and acetamiprid). Moreover, the effect of H_2O_2 addition is more significant for those EPs more reluctant to direct photolysis. This can be explained by considering two competitive photodegradation routes: direct photolysis and reaction with HO radicals generated from the photolysis of H_2O_2. Since a low rate of production of HO radicals is expected from the absorption coefficients of H_2O_2 above 280 nm [38], the contribution of indirect mechanisms to the overall degradation process is less significant for those EPs which show faster direct photolysis (amoxicillin, acetamiprid and clofibric acid). A similar trend was observed in the presence of 20 mg L^{-1} of CVT230, although lower rates were obtained for each EP, most probably due to the light screening effect and scavenging of HO radicals by SBO. These results (in absence and presence of H_2O_2) indicate that SBO are not effective as photosensitizers when pollutants have significant direct photolysis.

References

1. Montoneri, E., Mainero, D., Boffa, V., Perrone, D. G., & Montoneri, C. (2011). Biochemenergy: A project to turn an urban wastes treatment plant into biorefinery for the production of energy, chemicals and consumer's products with friendly environmental impact. *International Journal of Global Environmental Issues, 11*, 170–196.
2. Sutton, R., & Sposito, G. (2005). Molecular structure in soil humic substances: The new view. *Environmental Science and Technology, 39*, 9009–9015.
3. Kelleher, B. P., & Simpson, A. J. (2006). Humic substances in soils: Are they really chemically distinct? *Environmental Science and Technology, 40*, 4605–4611.
4. Quagliotto, P., Montoneri, E., Tambone, F., Adani, F., Gobetto, R., & Viscardi, G. (2006). Chemicals from wastes: Compost-derived humic acid-like matter as surfactant. *Environmental Science and Technology, 40*, 1686–1692.
5. Korshin, G. V., Li, C.-W., & Benjamin, M. M. (1997). Monitoring the properties of natural organic matter through UV spectroscopy: A consistent theory. *Water Research, 31*, 1787–1795.
6. Senesi, N., Miano, T. M., Provenzano, M. R., & Brunetti, G. (1989). Spectroscopic and compositional comparative characterization of I.H.S.S. reference and standard fulvic and humic acids of various origin. *Science of the Total Environment, 81–82*, 143–156.
7. Coble, P. G. (2007). Marine optical biogeochemistry: The chemistry of ocean color. *Chemical Reviews, 107*, 402–418.

8. Chen, Y., Senesi, N., & Schnitzer, M. (1977). Information provided on humic substances by E4/E6 ratios1. *Soil Science Society of America Journal, 41*, 352–358.
9. Lguirati, A., Ait Baddi, G., El Mousadik, A., Gilard, V., Revel, J. C., & Hafidi, M. (2005). Analysis of humic acids from aerated and non-aerated urban landfill composts. *International Biodeterioration and Biodegradation, 56*, 8–16.
10. Ma, J., Del Vecchio, R., Golanoski, K. S., Boyle, E. S., & Blough, N. V. (2010). Optical properties of humic substances and CDOM: Effects of borohydride reduction. *Environmental Science and Technology, 44*, 5395–5402.
11. Sharpless, C. M., & Blough, N. V. (2014). The importance of charge-transfer interactions in determining chromophoric dissolved organic matter (CDOM) optical and photochemical properties. *Environmental Science: Processes & Impacts, 16*, 654–671.
12. Thomas-Smith, T. E., & Blough, N. V. (2001). Photoproduction of hydrated electron from constituents of natural waters. *Environmental Science and Technology, 35*, 2721–2726.
13. Zepp, R. G., Braun, A. M., Hoigne, J., & Leenheer, J. A. (1987). Photoproduction of hydrated electrons from natural organic solutes in aquatic environments. *Environmental Science and Technology, 21*, 485–490.
14. Wang, W., Zafiriou, O. C., Chan, Iu Y, Zepp, R. G., & Blough, N. V. (2007). Production of hydrated electrons from photoionization of dissolved organic matter in natural waters. *Environmental Science and Technology, 41*, 1601–1607.
15. Grebel, J. E., Pignatello, J. J., & Mitch, W. A. (2011). Sorbic acid as a quantitative probe for the formation, scavenging and steady-state concentrations of the triplet-excited state of organic compounds. *Water Research, 45*, 6535–6544.
16. Bruccoleri, A., Pant, B. C., Sharma, D. K., & Langford, C. H. (1993). Evaluation of primary photoproduct quantum yields in fulvic acid. *Environmental Science and Technology, 27*, 889–894.
17. Zepp, R. G., Schlotzhauer, P. F., & Sink, R. M. (1985). Photosensitized transformations involving electronic energy transfer in natural waters: Role of humic substances. *Environmental Science and Technology, 19*, 74–81.
18. Paul, A., Hackbarth, S., Vogt, R. D., Röder, B., Burnison, B. K., & Steinberg, C. E. W. (2004). Photogeneration of singlet oxygen by humic substances: Comparison of humic substances of aquatic and terrestrial origin. *Photochemical & Photobiological Sciences, 3*, 273–280.
19. Dalrymple, R. M., Carfagno, A. K., & Sharpless, C. M. (2010). Correlations between dissolved organic matter optical properties and quantum yields of singlet oxygen and hydrogen peroxide. *Environmental Science and Technology, 44*, 5824–5829.
20. Garg, S., Rose, A. L., & Waite, T. D. (2011). Photochemical production of superoxide and hydrogen peroxide from natural organic matter. *Geochimica et Cosmochimica Acta, 75*, 4310–4320.
21. Page, S. E., Arnold, W. A., & McNeill, K. (2011). Assessing the contribution of free hydroxyl radical in organic matter-sensitized photohydroxylation reactions. *Environmental Science and Technology, 45*, 2818–2825.
22. Page, S. E., Sander, M., Arnold, W. A., & McNeill, K. (2012). Hydroxyl radical formation upon oxidation of reduced humic acids by oxygen in the dark. *Environmental Science and Technology, 46*, 1590–1597.
23. Rosario-Ortiz, F. L., Mezyk, S. P., Doud, D. F. R., & Snyder, S. A. (2008). Quantitative correlation of absolute hydroxyl radical rate constants with non-isolated effluent organic matter bulk properties in water. *Environmental Science and Technology, 42*, 5924–5930.
24. Miller, C. J., Rose, A. L., & Waite, T. D. (2012). Hydroxyl radical production by H_2O_2-mediated oxidation of Fe(II) complexed by Suwannee river fulvic acid under circumneutral freshwater conditions. *Environmental Science and Technology, 47*, 829–835.
25. Scully, N. M., Cooper, W. J., & Tranvik, L. J. (2003). Photochemical effects on microbial activity in natural waters: The interaction of reactive oxygen species and dissolved organic matter. *FEMS Microbiology Ecology, 46*, 353–357.
26. Bosio, G. N., David Gara, P. M., Einschlag, F. S., Gonzalez, M. C., Del Panno, M. T., & Martire, D. O. (2008). Photodegradation of soil organic matter and its effect on gram-negative bacterial growth. *Photochemistry and Photobiology, 84*, 1126–1132.

27. Aguer, J. P., Richard, C., & Andreux, F. (1997). Comparison of the photoinductive properties of commercial, synthetic and soil-extracted humic substances. *Journal of Photochemistry and Photobiology A: Chemistry, 103*, 163–168.
28. Halladja, S., ter Halle, A., Aguer, J.-P., Boulkamh, A., & Richard, C. (2007). Inhibition of humic substances mediated photooxygenation of furfuryl alcohol by 2,4,6-trimethylphenol. Evidence for reactivity of the phenol with humic triplet excited states. *Environmental Science and Technology, 41*, 6066–6073.
29. Bianco Prevot, A., Avetta, P., Fabbri, D., Laurenti, E., Marchis, T., Perrone, D. G., et al. (2011). Waste-derived bioorganic substances for light-induced generation of reactive oxygenated species. *ChemSusChem, 4*, 85–90.
30. Avetta, P., Bianco, P. A., Fabbri, D., Montoneri, E., & Tomasso, L. (2012). Photodegradation of naphthalene sulfonic compounds in the presence of a bio-waste derived sensitizer. *Chemical Engineering Journal, 197*, 193–198.
31. Bianco Prevot, A., Fabbri, D., Pramauro, E., Baiocchi, C., Medana, C., Montoneri, E., & Boffa, V. (2010). Sensitizing effect of bio-based chemicals from urban wastes on the photodegradation of azo-dyes. *Journal of Photochemistry and Photobiology A: Chemistry, 209*, 224–231.
32. Gomis, J., Vercher, R. F., Amat, A. M., Mártire, D. O., González, M. C., Bianco Prevot, A., et al. (2013). Application of soluble bio-organic substances (SBO) as photocatalysts for wastewater treatment: Sensitizing effect and photo-Fenton-like process. *Catalysis Today, 209*, 176–180.
33. Vione, D., Maurino, V., Minero, C., & Pelizzetti, E. (2001). Phenol photonitration upon UV irradiation of nitrite in aqueous solution I: Effects of oxygen and 2-propanol. *Chemosphere, 45*, 893–902.
34. Avetta, P., Bella, F., Bianco, A. P., Laurenti, E., Montoneri, E., Arques, A., & Carlos, L. (2013). Waste cleaning waste: Photodegradation of monochlorophenols in the presence of waste-derived photosensitizer. *ACS Sustainable Chemistry & Engineering, 1*, 1545–1550.
35. Tratnyek, P. G., & Hoigne, J. (1991). Oxidation of substituted phenols in the environment: A QSAR analysis of rate constants for reaction with singlet oxygen. *Environmental Science and Technology, 25*, 1596–1604.
36. Carlos, L., Mártire, D. O., Gonzalez, M. C., Gomis, J., Bernabeu, A., Amat, A. M., & Arques, A. (2012). Photochemical fate of a mixture of emerging pollutants in the presence of humic substances. *Water Research, 46*, 4732–4740.
37. Gomis, J., Bianco, A. P., Montoneri, E., González, M. C., Amat, A. M., Mártire, D. O., et al. (2014). Waste sourced bio-based substances for solar-driven wastewater remediation: Photodegradation of emerging pollutants. *Chemical Engineering Journal, 235*, 236–243.
38. García Einschlag, F. S., Carlos, L., Capparelli, A. L., Braun, A. M., & Oliveros, E. (2002). Degradation of nitroaromatic compounds by the UV-H_2O_2 process using polychromatic radiation sources. *Photochemical & Photobiological Sciences, 1*, 520–525.

Chapter 3
SBO in Water Detoxification: Photo-Fenton Processes at Mild Conditions

J. Gomis, M. Mora, R. Vicente, R. Vercher, A.M. Amat and A. Arques

Abstract The implementation of a photo-Fenton process at mild acidic conditions is a potential environmental application for SBOs. The Fenton reagent (sacrificial amounts of hydrogen peroxide and catalytic iron salts) has been demonstrated as an efficient method for the removal of toxic xenobiotics that is enhanced upon irradiation; sunlight can be used for this purpose. In order to avoid precipitation of iron at pH above 3, several strategies have been tested. One of them involves formation of photoactive iron complexes. Humic substances have been employed for this purpose, due to their ability to complex iron. Because of its similar chemical properties, SBO are candidates for this purpose. Experiments carried out with different pollutants have shown that SBO are not good photocatalysts because of the strong screen effect associated to their color, while they are useful to drive a photo-Fenton at milder pH, as they are good complexing agents for iron. Döehlert matrixes have been employed to determine that the pH range for efficient photo-Fenton can be extended to values of ca. 5 and that optimal SBO concentration is approximately 20 mg/L. Finally, SBO have demonstrated to be non toxic, scarcely biodegradable and relatively resistant to oxidizing conditions.

Keywords Soluble bio-organic substances · Wastewater treatment · Photocatalysis · Mild photo-Fenton · Process optimization

J. Gomis · R. Vicente · R. Vercher · A.M. Amat (✉) · A. Arques
Departamento de Ingeniería Textil y Papelera, Universidad Politécnica de Valencia, Campus de Alcoy Plaza Ferrándiz y Carbonell s/n, 03801, Alcoy, Spain
e-mail: aamat@txp.upv.es

A. Arques
e-mail: aarques@txp.upv.s

M. Mora
Departamento de Matemática Aplicada, Universidad Politécnica de Valencia, Campus de Alcoy, Plaza Ferrándiz y Carbonell s/n, 03801, Alcoy, Spain

A. Arques and A. Bianco Prevot (eds.), *Soluble Bio-based Substances Isolated From Urban Wastes*, SpringerBriefs in Green Chemistry for Sustainability,
DOI 10.1007/978-3-319-14744-4_3

3.1 Introduction

Oxidative photochemical processes for wastewater treatment have been demonstrated as a promising alternative to deal with those effluents which cannot be treated by conventional means, such as those containing toxic or non-biodegradable compounds [1]. These processes are based in the generation "in situ" of highly reactive species, such as hydroxyl radical or singlet oxygen. For this purpose, irradiation in the UV-vis range is required. In some cases, the presence of a photocatalyst is also needed [2].

The use of sunlight as irradiation source is especially attractive, because of the economic and ecologic advantages that are involved [3, 4]. However, only radiation with wavelengths above 300 nm reaches the Earth's surface, meaning that it is limited to those photocatalysts that are efficient in the UVA-visible range of the spectrum. Among the systems that fulfill these conditions are some semiconductor solids (in particular titanium dioxide) [5], photoactive organic molecules [6] and processes based in the Fenton reagent [7].

The photo-Fenton process has been demonstrated to be among the most efficient ones that can be driven under UVA-visible light. Briefly, it consists in a combination of iron salts and hydrogen peroxide: iron cation catalyzes the decomposition of the peroxide into more reactive species, mainly hydroxyl radical (·OH), following a process that is greatly accelerated by irradiation. Although the mechanism is very complex, it is still not completely elucidated and might depend on the experimental conditions, it can be simplified in two main reactions (Eqs. 3.1–3.2):

$$Fe^{2+} + H_2O_2 \rightarrow Fe^{3+} + OH^- + \cdot OH \tag{3.1}$$

$$Fe(OH)^{2+} + h\nu \rightarrow Fe^{2+} + \cdot OH \tag{3.2}$$

The better performance of photo-Fenton when compared with dark Fenton is mainly due to Eq. 3.2. In fact, $Fe(OH)^{2+}$ is decomposed, resulting in a photoreduction of iron(III) to iron(II) and the generation of further amounts of ·OH. The key role of $Fe(OH)^{2+}$ also explains the acidic pH required by photo-Fenton, namely 2.8, because under this conditions, formation of the photo-active iron complex is favoured. On the other hand, at higher pH values, iron can be predominantly found as oxide or hydroxide, which are not active for the photo-Fenton process.

3.2 Towards Photo-Fenton at Mild pH Conditions

The highly acidic pH required by photo-Fenton is one of its major disadvantages, as for most effluents acid addition is required, followed by a neutralization before it can be discharged. Hence, modifications of the Fenton reagent and the photo-Fenton

process to allow its implementation at milder pH conditions have deserved attention from researchers, and different strategies have been followed for this purpose.

The use of the small fraction of iron that remains soluble at circumneutral medium has been investigated to deal with pollutants at low concentrations, such as xenobiotics at the outlet of wastewater treatment plants. These chemicals reach concentrations which ranges from ng/L to a few μg/L. For this reason a short treatment time, in which some iron might still remain is solution, should be enough to treat this effluent. This strategy has been applied to treat real effluents [8, 9] or aqueous samples spiked with those compounds [10].

Another possibility is the use of iron in heterogeneous phase. In this context, zero valent iron has been employed at mild pH values. In this process, iron is oxidized to form in situ iron cations, which, in turn, drive the (photo)-Fenton like process [11]. Other ways to heterogeneous the process is supporting the iron cation onto different solids such as zeolites [12] of films [13].

An alternative strategy, which has been more widely studied, consists in the use of compounds able to prevent the formation of iron oxides or hydroxides, commonly by forming photochemically active complexes. The ability of some carboxylates, such as oxalate, to enhance the photo-Fenton process is well established [14]. Recently, complexes between iron and organic ligands such as citrate [15, 16], ethylenediamine-N,N′-disuccinic acid (EDDS) [17, 18] or EDTA [19] have been demonstrated to be able to extend the pH range of photo-Fenton until values above 5. In some cases, a modification of the mechanism has been proposed under such conditions, attributing a key role in the process to other species different to hydroxyl radical, such as superoxide [17, 20]. Despite the good performance shown in some cases, this approach is not free of inconveniences, namely the limited stability of the employed complexing agent and the potential toxicity of those chemical auxiliaries.

Humic substances (HS) are also candidates for the implementation of photo-Fenton at mild pH. HS are naturally occurring macromolecules which are mainly originated from plant debris and are the most widely distributed organic materials in the environment [21]. These substances contain functional groups that are able to complex iron [22]. This ability has been successfully employed in the removal of chemicals by dark Fenton process [23, 24], which has been extended to a pH range of 5–8 [25]. A complex formed between iron and the humic substances has been proposed as the key species driving the process.

Although the role of HS in photo-Fenton process has not been widely studied, there is some information on its use in solar driven processes to remove pollutants at low concentration at the outlet of a wastewater treatment plant [26]. A recent paper published by our research group has demonstrated that these substances show a positive effect on a solar-simulated photo-Fenton process at pH = 7.2 using a mixture of pharmaceuticals and pesticides (at an initial concentration of 5 mg/L each) as target effluent [10]. Table 3.1 shows the percentage of removal achieved after 180 min of irradiation in a solar simulator with and without humic substances. In the presence of HS, three pollutants were totally removed after three hours of irradiation, more than 80 % removal was achieved for other two,

Table 3.1 Photodegradation (%) of a mixture of 6 pollutants (initial concentration 5 mg/L each) under simulated sunlight

Pollutant	With HS (%)	Without HS (%)
Amoxicillin	>99	77
Acetaminophen	>99	49
Acetemiprid	46	24
Caffeine	82	36
Clofibric acid	>99	93
Carbamazepine	90	53

and acetamiprid was the most reluctant, as only 46 % of photodegradation was reached. The efficiency of the process without HS was significantly lower, as only for clofibric acid removal was above 80 %. Nevertheless, those results are far away those obtained at pH = 2.8, as under those conditions, the complete abatement of all six pollutants was reached in a few minutes.

By contrast, when the concentration of those pollutants was lower (several μg/L) HS played a negative role, most probably due to a competitive effect of HS towards the target pollutants. This effect has already been observed by other authors [27], showing that the actual effect of dissolved organic matter on the photo-Fenton process might strongly depend on the experimental conditions, thus explaining the discrepant results shown in literature.

Regarding to the mechanistic studies, results are not concluding, as expectable for such a complex system. However, it has been reported that ·OH radical might not be the only species involved in the process and hence, other oxidizing species might be responsible for the pollutants oxidation [28].

3.3 Photo-Fenton Process Based on SBOs: Decoloration of Crystal Violet

Soluble bio-organic substances (SBO) extracted from the humid fraction of organic solid wastes are an attractive alternative to HS. As described in Chap. 1, the structure of these substances has been described to be similar to that of humic acids and hence, chemical and physical characteristics are not expected to be very different. In fact, results shown in Chap. 2 indicate that SBO, as happens with HS, are able to generate reactive species upon UV/visible irradiation. However, its actual applicability as photocatalyst for wastewater treatment is limited by its dark colour, which results in an important screen effect which is detrimental for the photocatalytic activity.

However, the functional groups present in the structure of SBO (e.g. carboxylic or amide) indicate that these substances are able to act as chelating agents for iron, what might be useful to apply photo-Fenton at neutral conditions. As a matter of fact, SBO contain significant amount of iron in its

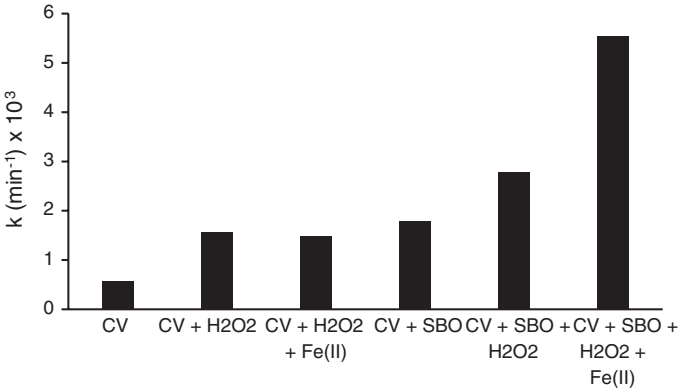

Fig. 3.1 Pseudo-first order rate constant obtained in the decoloration of crystal violet solutions (initial CV concentration = 10 mg/L) at neutral pH under medium pressure mercury lamp irradiation ($\lambda > 300$ nm) with or without the following chemicals: $[H_2O_2] = 8.3$ mg/L; [Fe(II)] = 5 mg/L; [SBO] = 100 mg/L

composition (0.1–0.8 %, ca. 0.7 % in the case of CVT230), and hence, they might be expected to drive a photo-Fenton-like process, even without iron addition. In order to clarify this point, decoloration of crystal violet (CV), a cationic dye, has been studied in the presence of SBO (CVT 230) [29]. Figure 3.1 shows the pseudo first order rate constants measured for decoloration of CV, a cationic dye, under different experimental conditions, combining SBO, Fe(II), H_2O_2 with CV at neutral pH.

Results indicate that although CV suffered some photolysis, it was very low ($k < 10^{-3}$ min^{-1}). Addition of H_2O_2 or SBO resulted in some enhancement in the process, with k slightly below 2×10^{-3} min^{-1}; similar results were obtained with the Fenton reagent in the absence of SBOs (CV + H_2O_2 + Fe(II)). On the other hand, the combination of hydrogen peroxide and SBO was able to accelerate the decoloration of CV; this might be attributable to a photo-Fenton-like process at neutral pH in which the iron present in the SBO composition is involved. Addition of extra amounts of iron (5 mg/L) to the SBO/H_2O_2 mixture was still able to increase the reaction rate, indicating that only the iron present in the SBO is not able to drive an efficient photo-Fenton but these substances can stabilize iron in the medium, forming photochemically active species, most probably SBO-Fe complexes.

Regarding to the possible involvement of reactive species, experiments were carried out with different chemical probes. 2-propanol, a scavenger of hydroxyl radical, had a scarce effect on the decoloration rate of CV; this is in agreement with an alternative species to ·OH playing an important role in the process. On the other hand, addition of phenol resulted in a decrease of the reaction rate; as phenol inhibits processes involving ferryl ion, which might indicate that highly oxidized iron species becomes more predominating under those conditions.

3.4 Photo-Fenton Process Based on SBOs. Effect of Operational Parameters

SBO-driven photo-Fenton processes were also tested using a target effluent consisting of a mixture of six pollutants of environmental relevance, namely acetaminophen (analgesic), caffeine (stimulating agent), acetemiprid (insecticide), clofibric acid (metabolite of clofibrate, also employed as herbicide), carbamazepine (psychiatric drug) and amoxycillin (antibiotic) at a concentration of 5 mg/L each [30]. Irradiations were performed with a solar simulator, whose emission spectrum closely matches that of sunlight arriving at the Earth's surface.

First, the effect of SBO was tested at two different pH values, namely 2.8 and 5.3. For this purpose the photo-Fenton process (5 mg/L of iron, 75 mg/L of H_2O_2) was performed with and without SBO and the pseudo-first order rate constant was calculated in both cases; the ratio between the rate constant obtained in the presence of SBO (k_{SBO}) and in its absence (k_0); data are shown in Table 3.2.

Ratios were systematically well above 1 (ca. 8 in most cases) at the pH = 5.3 showing that the SBO was able to accelerate significantly the photo-Fenton process, most probably due to its ability to increase the availability of photochemically active iron species by preventing formation of iron oxides or hydroxydes. However, at pH = 2.8, ratios were slightly below 1, indicating that the role of SBO was detrimental. At this pH, precipitation of iron does not occur and hence the presence of SBO does not result in an extra generation of reactive species. On the contrary, this organic substance competes with the pollutants for the oxidizing species and might also produce some screen effect, decreasing the amounts of photons reaching the photocatalyst.

The effect of some operational variables, namely pH, SBO concentration and iron concentration was investigated using an experimental design methodology based on Doehler array [31]. The mixture of pollutants above described (5 mg/L each) was irradiated with a solar simulator in the presence of SBO (between 15 and 25 mg/L), iron(III) (2–6 mg/L) at pH values in the range 3–7. The concentration of hydrogen peroxide was half the stoichiometric amount required to mineralize the pollutants [32]. The response was the time required to decrease the concentration of each pollutant to one half of the initial value ($t_{50\%}$).

Table 3.2 Ratio between the pseudo-first order rate constant obtained for the photodegradation of 6 pollutants in the presence of SBO (k_{SBO}) and in its absence (k_0) at pH = 2.8 and 5.3

	k_{SBO}/k_0 at pH = 2.8	k_{SBO}/k_0 at pH = 5.3
Acetaminophen	0.73	8.81
Caffeine	0.77	8.43
Amoxicillin	0.87	6.15
Acetamiprid	0.65	8.37
Carbamazepine	0.75	8.75
Clofibric acid	0.88	8.28

A three dimensional surface response was obtained for each pollutant, which can be observed in Eqs. 3.3–3.8, where [Fe] and [SBO] are expressed as mg/L and $t_{50\%}$ in min:

$$\begin{aligned} t_{50\%}\,(\text{carbamazepine}) = {} & 248.38 - 40.37 \cdot [\text{Fe}] - 8.52 \cdot [\text{SBO}] - 51.39 \cdot \text{pH} \\ & + 1.90 \cdot [\text{Fe}]^2 + 0.07\,[\text{Fe}]\,[\text{SBO}] + 5.14 \cdot [\text{Fe}] \cdot \text{pH} \\ & + 0.43\,[\text{SBO}]^2 - 2.08 \cdot [\text{SBO}] \cdot \text{pH} + 10.28 \cdot \text{pH}^2 \end{aligned} \quad (3.3)$$

$$\begin{aligned} t_{50\%}\,(\text{acetominophen}) = {} & 318.33 - 5.36 \cdot [\text{Fe}] - 22.79 \cdot [\text{SBO}] - 32.82 \cdot \text{pH} \\ & + 0.82 \cdot [\text{Fe}]^2 + 0.30\,[\text{Fe}]\,[\text{SBO}] + 0.50\,[\text{Fe}]\,\text{pH} \\ & + 0.45\,[\text{SBO}]^2 + 0.71 \cdot [\text{SBO}] \cdot \text{pH} + 3.64 \cdot \text{pH}^2 \end{aligned} \quad (3.4)$$

$$\begin{aligned} t_{50}\,(\text{amoxicillin}) = {} & 56.92 - 41.63 \cdot [\text{Fe}] + 3.80 \cdot [\text{SBO}] - 19.34 \cdot \text{pH} + 1.28 \cdot [\text{Fe}]^2 \\ & + 0.08\,[\text{Fe}]\,[\text{SBO}] + 6.23 \cdot [\text{Fe}] \cdot \text{pH} + 0.36\,[\text{SBO}]^2 \\ & - 4.19 \cdot [\text{SBO}] \cdot \text{pH} + 10.69 \cdot \text{pH}^2 \end{aligned} \quad (3.5)$$

$$\begin{aligned} t_{50\%}\,(\text{acetamiprid}) = {} & 966.42 - 83.28 \cdot [\text{Fe}] - 40.02 \cdot [\text{SBO}] - 206.76 \cdot \text{pH} \\ & + 1.19 \cdot [\text{Fe}]^2 + 0.91 \cdot [\text{Fe}] \cdot [\text{SBO}] + 12.29 \cdot [\text{Fe}] \cdot \text{pH} \\ & + 0.69 \cdot [\text{SBO}]^2 + 1.77 \cdot [\text{SBO}] \cdot \text{pH} + 18.59 \cdot \text{pH}^2 \end{aligned} \quad (3.6)$$

$$\begin{aligned} t_{50\%}\,(\text{clofibric acid}) = {} & 242.78 - 40.30 \cdot [\text{Fe}] - 9.39 \cdot [\text{SBO}] - 44.58 \cdot \text{pH} \\ & + 1.44 \cdot [\text{Fe}]^2 + 0.13\,[\text{Fe}]\,[\text{SBO}] + 5.70 \cdot [\text{Fe}] \cdot \text{pH} \\ & + 0.44\,[\text{SBO}]^2 - 2.06 \cdot [\text{SBO}] \cdot \text{pH} + 9.40 \cdot \text{pH}^2 \end{aligned} \quad (3.7)$$

$$\begin{aligned} t_{50\%}\,(\text{caffeine}) = {} & 702.53 - 79.39 \cdot [\text{Fe}] - 25.36 \cdot [\text{SBO}] - 147.13 \cdot \text{pH} \\ & + 2.02 \cdot [\text{Fe}]^2 + 0.41\,[\text{Fe}]\,[\text{SBO}] + 12.04 \cdot [\text{Fe}] \cdot \text{pH} \\ & + 0.50 \cdot [\text{SBO}]^2 + 0.65\,[\text{SBO}]\,\text{pH} + 12.44 \cdot \text{pH}^2\,(\text{caffeine}) \end{aligned} \quad (3.8)$$

As expectable, pH was the most significant parameter. This effect can be better appreciated by means of a 2D-plot which can be obtained by fixing one of the three variables. Figure 3.2 shows, as an example, the contour lines obtained for carbamazepine at a concentration of SBO of 15 mg/L. It can be observed that that $t_{50\%}$ did not change significantly in the pH range 3–5 (highlighted in yellow in the figure) and iron concentration did not have a remarkable effect on the photo-Fenton process. Similar plots can be obtained for the other pollutants. This involves that SBO are useful auxiliaries to extend the photo-Fenton process until pH values close to 5.

Interestingly, the contour plot obtained in some cases (e.g. carbamazepine at high SBO concentration, namely 25 mg/L), shows a shift of the optimal pH domain towards higher values (close or even above 4). This might indicate that

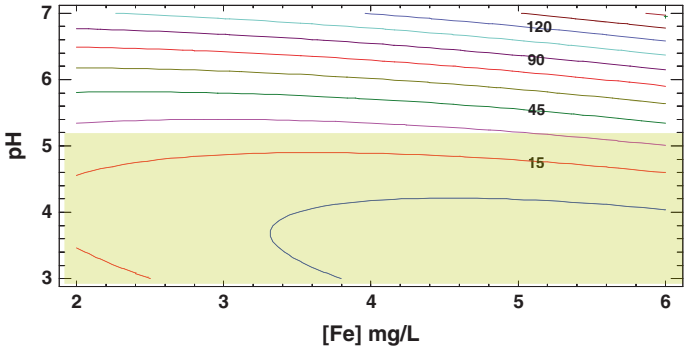

Fig. 3.2 Contour plot for $t_{50\%}$ (min) obtained for the photo-Fenton degradation of carbamazepine in the presence of 15 mg/L of SBO. The area where photo-Fenton is more efficient is highlighted in *yellow*

there is a modification of the photo-Fenton mechanism, where $Fe(OH)^{2+}$, which reaches its maximum concentration at pH = 2.8, is replaced as the key species, most probably by a Fe-SBO complex, as reported above.

If the pH is fixed at the value of 5, the effect of iron and SBO concentration can be studied. The concentration of iron in the studied range (2–6 mg/L) had no significant effect on the degradation rate. On the other hand, best results were reached with SBO concentration slightly above 20 mg/L, beyond this point, SBO played a negative role, either for the screen effect or as scavengers of the reactive species, competing with the pollutants.

The type of SBO might also be of importance for the photo-Fenton process. In order to check this point, the photo-Fenton process was driven with the mixture of six pollutants. Three different types of SBO, depending on its origin, were employed: (a) FORSUD, isolated from the urban waste organic fraction, mixed with the digestate from an anaerobic reactor; (b) CVT230, obtained from trimming residues aerated for 230 days and (c) CVDFT110, isolated from a mixture 35/55/10 (w/w/w) of FORSUD, trimming residues and urban sewage sludge mix, aerated for 110 days (see Chap. 1 for more information). Some characteristics are summarized in Table 3.3.

Table 3.3 Main characteristics of the SBOs employed in these studies

	FORSUD	CVDFT110	CVT230
Carbon (%, w/w)	45.1	35.5	38.2
Aliphatic carbon	43	31	37
Carboxylic	7	9	12
Lipophilic/hydrophilic ratio	9.3	5.3	3.6
Aliphatic/aromatic ratio	3.3	1.3	1.8
E_2/E_3 ratio	3.83	2.31	2.38

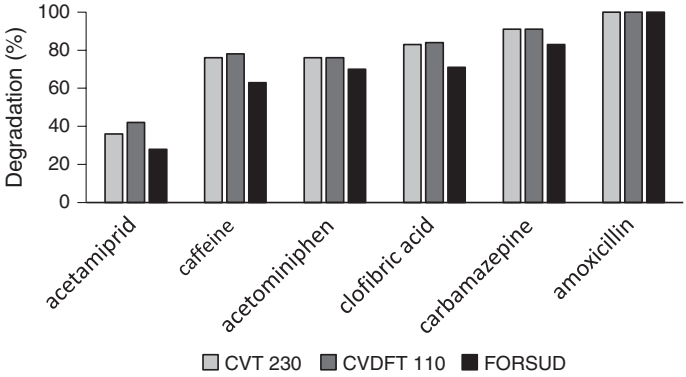

Fig. 3.3 Percentage of photodegradation of six pollutants achieved after 5 min of a photo-Fenton process in the presence of three different types of SBO

The photodegradation of all six pollutants was studied using all three types of SBOs. The percentage of photodegradation reached after 5 min of photo-Fenton treatment at pH = 5.2 was calculated for each pollutant and SBO (Fig. 3.3). It can be observed that the order of reactivity of the pollutants did no depend on the SBO that was employed. However, some quantitative differences can be observed among the SBO: while CVDFT110 and CVT230 showed a similar performance, that of FORSUD was clearly worse. Thus was attributed to differences in the composition, as in FORSUD, aliphatic carbon, which is not photochemically active and unable to keep iron in solution; on the other hand, carboxylic group, able to complex iron, is present at lower extent in FORSUD.

3.5 Biocompatibility and Stability of the SBO

Finally, for technical reasons, it is interesting to determine the toxicity, biodegradability and stability of the SBOs. In order to check toxicity, three different bioassays were performed, using bacteria (*V. fischeri*), algae (*P. subcapitata*) and crystals (*D. magna*). The toxicity was very low in all cases at the concentrations which were optimal in a photo-Fenton process (ca. 20 mg/L), as it was below 10 "for all essays and for every SBO at this concentration [32]. The biocompatibility of these substances was very low, as indicated by the biological oxygen demand/chemical oxygen demand ratio (BOD/COD), which was below 0.1, while the limit for a good biodegradability is commonly considered to be ca. 0.4.

The effect of photochemical treatments on the SBOs was investigated. For this purpose, they were irradiated in the presence of the stoichiometric amount of H_2O_2 to mineralize these compounds. Once the sample was free of H_2O_2, it was analyzed. Data obtained before and after irradiation are shown in Table 3.4. This table shows that there was a moderate mineralization of the samples as shown by

Table 3.4 Irradiation of CVT230 in the presence of hydrogen peroxide: main parameters before and after irradiation

	Before irradiation	After irradiation
DOC (mg/L)	28.2	23.5
COD (mg/L)	95	63
BOD/COD	0.04	0.14
Surface tension	69	73
E_2/E_3 ratio	2.38	3.89

DOC decrease (20–30 %), some oxidation, indicated by the variation of COD an slight enhancement of the biodegradability shown by the BOD/COD ratio, surface tension increased to reach values close to that of distilled water and the E_2/E_3 ratio significantly increased. All these results are in agreement with a cleavage of the starting SBO to release smaller, more oxidized and more hydrophilic substances.

3.6 Summary and Outlook

Advanced oxidation processes for wastewater treatment is a potential use of SBO extracted from urban wastes. Despite the photo-activity of these substance, their use as photocatalysts should be disregarded, as they are not able to enhance the photodegradation of xenobiotics under simulated sunlight. On the other hand, these substances might be useful to drive a photo-Fenton at mild acidic conditions because of their ability to complex iron. However, before this technology can be applied, more research is needed in order to check the performance of the process under sunlight and to optimize operational parameters under real situations. Economic evaluation is also required.

Gaining further insight into the mechanism of the process seems also interesting, despite the complexity of the system. Determination of the nature of the complex between SBO and iron or the key reactive species involved in the process, and variation of the SBO composition during oxidation seems meaningful.

Finally, developing of SBO form different origins, less coloured and showing an improved photochemical activity might also contribute to enhance their applicability.

References

1. Oller, I., Malato, S., & Sánchez-Pérez, J. A. (2011). Combination of advanced oxidation processes and biological treatments for wastewater decontamination—a review. *Science of the Total Environment, 409*(4141), 4146.
2. Legrini, O., Oliveros, E., & Braun, A. M. (1994). Photochemical processes for water treatment. *Chemical Reviews, 93*(671), 698.
3. Malato, S., Blanco, J., Vidal, A., & Richter, C. (2002). Photocatalysis with solar energy at a pilot-plant scale: An overview. *Applied Catalysis B: Environmental, 37*, 1–15.

4. Malato, S., Fernández-Ibáñez, P., Maldonado, M. I., Blanco, J., & Gernjak, W. (2009). Decontamination and disinfection of water by solar photocatalysis: Recent overview and trends. *Catalysis Today, 147*, 1–59.
5. Gaya, U. I., & Abdullah, A. H. (2008). Heterogeneous photocatalytic degradation of organic contaminants over titanium dioxide: A review of fundamentals, progress and problems. *Journal of Photochemistry and Photobiology C: Photochemistry Reviews, 9*, 1–12.
6. Marín, M. L., Arques, A., Santos-Juanes, L., Amat, A. M., & Miranda, M. A. (2012). Organic photocatalysis for the oxidation of pollutants and model compounds. *Chemical Reviews, 112*, 1710–1750.
7. Pignatello, J. J., Oliveros, E., & Mackay, A. (2006). Advanced oxidation processes for organic contaminant destruction based on the Fenton reaction and related chemistry. *Critical Reviews in Environmental Science and Technology, 36*, 1–84.
8. Klamerth, N., Rizzo, L., Malato, S., Maldonado, M. I., Agüera, A., & Fernández-Alba, A. (2010). Degradation of fifteen emerging contaminants at 1 $\mu g\ L^{-1}$ initial concentrations by mild solar photo-Fenton in MWTP effluents. *Water Research, 44*, 545–554.
9. Bernabeu, A., Vercher, R. F., Santos-Juanes, L., Simón, P. J., Lardín, C., Martínez, M. A., et al. (2011). Solar photocatalysis as a tertiary treatment to remove emerging pollutants from wastewater treatment plant effluents. *Catalysis Today, 161*, 233–240.
10. Bernabeu, A., Palacios, S., Vicente, R., Vercher, R. F., Malato, S., Arques, A., & Amat, A. M. (2012). Solar photo-Fenton at mild conditions to treat a mixture of six emerging pollutants. *Chemical Engineering Journal, 198–199*, 65–72.
11. Nie, J., Hu, C., Qu, J., Zhou, L., & Hu, X. (2007). Photoassisted degradation of azo dyes over FexH2x-3/Fe0 in the presence of H_2O_2 at neutral values. *Environmental Science and Technology, 41*, 4715–4719.
12. Fukuchi, S., Nishimoto, R., Fukushima, M., & Zhu, Q. (2014). Effects of reducing agents on the degradation of 2,4,6-tribromophenol in a heterogeneous Fenton-like system with an iron-loaded natural zeolite. *Applied Catalysis B: Environmental, 147*, 411–419.
13. Mazille, F., Schoettl, T., Klamerth, N., Malato, S., & Pulgarin, C. (2010). Field solar degradation of pesticides and emerging water contaminants mediated by polymer films containing titanium and iron oxide with synergistic heterogeneous photocatalytic activity at neutral pH. *Water Research, 44*, 3029–3038.
14. Monteagudo, J. M., Durán, A. M., & López-Almodóvar, C. (2008). Homogeneous ferrioxa-late-assisted solar photo-Fenton degradation of Orange II aqueous solutions. *Applied Catalysis B: Environmental, 83*, 46–55.
15. Hong, J., Lu, S., Zhang, C., Qi, S., & Wang, Y. (2011). Removal of Rhodamine B under visible irradiation in the presence of Fe^0, H_2O_2, citrate and aeration at circumneutral pH. *Chemosphere, 84*, 1542–1547.
16. Silva, M. R. A., Trovó, A. G., & Nogueira, R. F. P. (2007). Degradation of the herbicide tebuthiuron using solar photo-Fenton process and ferric citrate complex at circumneutral pH. *Journal of Photochemistry and Photobiology A: Chemistry, 191*, 187–192.
17. Huang, W., Brigante, M., Wu, F., Hanna, K., & Mailhot, G. (2013). Effect of ethylenediamine-N, N'-disuccinic acid on Fenton and photo Fenton processes using goethite as an iron source: Optimization of parameters for bisphenol A degradation. *Environmental Science and Pollution Research, 20*, 39–50.
18. Klamerth, N., Malato, S., Agüera, A., & Fernández-Alba, A. R. (2013). Photo-Fenton and modified photo-Fenton at neutral pH for the treatment of emerging contaminants in wastewater treatment plant effluents: A comparison. *Water Research, 47*, 833–840.
19. De Luca, A., Dantas, R. F., & Esplugas, S. (2014). Assessment of iron chelates efficiency for photo-Fenton at neutral pH. *Water Research, 61*, 232–242.
20. Hug, S. J., & Leupin, O. (2003). Iron-catalyzed oxidation of arsenic(III) by oxygen and by hydrogen peroxide: pH-dependent formation of oxidants in the Fenton reaction. *Environmental Science and Technology, 37*, 2734–2742.

21. Chin, Y. P., Aiken, G., & O'Loughlin, E. (1994). Molecular weight, polydispersity, and spectroscopic properties of aquatic humic substances. *Environmental Science and Technology, 28*, 1853–1858.
22. Mikutta, C., & Kretzschmar, R. (2011). Spectroscopic evidence for ternary complex formation between arsenate and ferric iron complexes of humic substances. *Environmental Science and Technology, 45*, 9550–9557.
23. Lipczynska-Kochany, E., & Kochany, J. (2008). Effect of humic substances on the Fenton treatment of wastewater at acidic and neutral pH. *Chemosphere, 73*, 745–750.
24. Georgi, A., Schierz, A., Trommler, U., Horwitz, C. P., Collins, T. J., & Kopinke, F. D. (2007). Humic modified Fenton reagent for enhancement of the working pH range. *Applied Catalysis B: Environmental, 72*, 26–36.
25. Fan, C., Tsui, L., & Liao, M. (2011). Parathion degradation and its intermediate formation by Fenton process in neutral environment. *Chemosphere, 82*, 229–236.
26. Klamerth, N., Malato, S., Maldonado, M. I., Agüera, A., & Fernández-Alba, A. R. (2011). Modified photo-Fenton for degradation of emerging contaminants in municipal wastewater effluents. *Catalysis Today, 161*, 241–246.
27. Khan, J. A., He, X., Khan, H. M., Shah, N. S., & Dionysiou, D. D. (2013). Oxidative degradation of atrazine in aqueous solution by UV/H_2O_2/Fe^{2+} and UV/HSO^{5-}/Fe^{2+} processes: A comparative study. *Chemical Engineering Journal, 218*, 376–383.
28. Vermilyea, W., & Voelker, B. M. (2009). Photo-Fenton reaction at near neutral pH. *Environmental Science and Technology, 43*, 6927–6933.
29. Gomis, J., Vercher, R. F., Amat, A. M., Mártire, D. O., González, M. C., Bianco Prevot, A., et al. (2013). Application of soluble bio-organic substances (SBO) as photocatalysts for wastewater treatment: Sensitizing effect and photo-Fenton-like process. *Catalysis Today, 209*, 176–180.
30. Gomis, J., Bianco Prevot, A., Montoneri, E., González, M. C., Amat, A. M., Mártire, D. O., et al. (2014). Waste sourced bio-based substances for solar-driven wastewater remediation: Photodegradation of emerging pollutants. *Chemical Engineering Journal, 235*, 236–243.
31. Ferreira, S. L. C., dos Santos, W. N. L., Quintella, C. M., Neto, B. B., & Bosque-Sendra, J. M. (2004). Doehler matrix: A chemometric tool for analytical chemistry. *Review Talanta, 63*, 1061–1067.
32. Gomis, J., Carlos, L., Bianco-Prevot, A., Teixeira, A. C. S. C., Mora, M., Amat, A. M., et al. (2014). Bio-based substances from urban waste as auxiliaries for solarphoto-Fenton treatment under mild conditions: Optimization of operational variables. *Catalysis Today*. doi:10.1016/j.cattod.2014.03.034.

Chapter 4
Effect of Humic Substances and Bioorganic Substrates from Urban Wastes in Nanostructured Materials Applications and Synthesis

G. Magnacca, E. Laurenti and M.C. Gonzalez

Abstract Humic substances were widely studied for preparing materials to be used for adsorption, photocatalysis and so on. Their parent soluble bio-organic materials (SBO) have potentially similar applications which have to be evaluated. The main advantage of the use of SBO substances concerns their low cost, but they are appealing also for the development of a strategy of recycle and reuse of wastes which needs to be followed worldwide. The application of SBO in materials synthesis is promizing, since they can be used as synthesis intermediates but also as active phases for developing adsorbing and/or photoactive materials usable for environmental applications.

Keywords Material synthesis · Physico-chemical characterization · Humic substances · Adsorption · Photocatalysis

4.1 Introduction

Humic substances (HS) and their similar soluble bio-organic materials (SBO) obtained from urban green wastes were suggested as efficient, cost-effective, and environmentally friendly alternative to existing materials, particularly those used in pollution treatment [1–3].

G. Magnacca · E. Laurenti
Dipartimento di Chimica and NIS Centre, Università di Torino, Via P. Giuria 7, 10125 Torino, Italy

M.C. Gonzalez (✉)
Instituto de Investigaciones Fisicoquímicas Teóricas y Aplicadas (INIFTA), CCT-La Plata-CONICET, Universidad Nacional de La Plata, La Plata, Argentina
e-mail: mcgonzalez.quim@gmail.com

A. Arques and A. Bianco Prevot (eds.), *Soluble Bio-based Substances Isolated From Urban Wastes*, SpringerBriefs in Green Chemistry for Sustainability,
DOI 10.1007/978-3-319-14744-4_4

In particular, HS are used as sorbents of different metals due to their large number of functional groups capable of binding metal ions. Their efficiency for the removal of heavy metals strongly depends on the HS origin, as demonstrated in recent studies with different HS samples: peat, aquatic, and industrial, tested as sorbents for the removal of zinc(II), iron(III), and bismuth(III)-oxides nanoparticles [1].

HS sorption on nanomaterials surface is also of importance and of actual environmental concern. Because of their widespread application, manufactured nanomaterials are being produced in very large quantities and thus require environmental impact assessment to reduce environmental risks in case of their releases and possible pollution. It is almost inevitable that they will end up in the aquatic environment where they may adsorb HS.

4.2 HS-Adsorbed Nanomaterials

The HS-adsorbed nanomaterials may show different surface properties, fate, transportation, and aggregation than those of the original nanoresidues. Also, the nanomaterials stability is of significance in determining their bioavailability and toxicity. The major mechanisms of adsorption by natural organic matter have been proposed to involve [4] (i) anion exchange (electrostatic interaction), (ii) ligand exchange, (iii) hydrophobic interaction, (iv) entropic effect, (v) hydrogen bonding, and (vi) cation bridging. Changes in the form and microstructure of HA (humic acids) depend on the pH, concentration, and ionic strength of the aqueous solutions. At low pH and high ionic strength, HA aggregation through van der Waals forces into spherical agglomerates is observed. On the other hand, in alkaline solutions, HA acidic groups are dissociated and do not form aggregates due to coulomb repulsion. Therefore, both, HA adsorption characteristics and substrate surface chemistry and charge, strongly depend on pH. As a consequence, HA adsorption on nanomaterials and its environmental impact cannot be generalized due to a complex pH and material-dependent behavior.

Among the altered properties, aggregation is critical for characterizing transportation of nanomaterials in the environment. For example, addition of HS to aqueous suspensions of oxide and metallic nanomaterials such as ZnO, TiO_2, Fe_2O_3, NiO, γ-Al_2O_3, and Ag decreases the propensity of these nanoparticles to aggregate because HS greatly increase the negative surface charge of the particles [5, 6]. Interestingly, high HA adsorption by nanosized TiO_2 and γ-Al_2O_3 could be attributed to the electrostatic attraction and ligand exchange of HA phenolic OH and COOH groups at the particles large positively-charged surfaces. On the other hand, the low hydrophilic surface of negatively-charged nano-ZnO was suggested to be responsible for HA adsorption. SiO_2 nanoparticles remain stable independently of the presence of humic and fulvic acids at pH 5 and 25 °C because of their high hydrophilicity and large number of negative surface charges which limit the adsorption capacity of natural organic matter [7]. Adsorption of HA decreases the micropore surface area of nano-oxides but not the external area due

to micropore blockage. HA-coated nano-oxides could be more easily dispersed and suspended and more stable in solution than uncoated ones because of their enhanced electrostatic repulsion.

In acidic conditions, HA may behave as a surfactant forming composite material to negatively-charged surfaces as montmorillonite. Protonated HA aggregates incorporate negatively-charged silicate layers of Na-montmorillonite yielding spherical aggregates with microstructural characteristics consisting of HA and extremely thin fragments of montmorillonite [8]. The decreased intensity and increased line broadening observed for the XRD patterns of these composites support a disordering of the montmorillonite stacking sequence and its cleavage into silicate layers. The electron diffraction (ED) patterns further support namontmorillonite layer isolation as they show almost no observable diffraction pattern. Formation of isolated silicate layers was attributed to the chelating ability of HA. On the other hand, montmorillonite-HA composites formed at pH 12 are of similar form and microstructure than that of alkali treated montmorillonite. TEM images show that these composites look like thin ribbons or plates with turbostratic layering of the silicate layers [8].

A pH-dependent adsorption of HA on magnetite is also reported [9]. The isoelectric point (IEP) of magnetite was observed at pH ~8, where large aggregates are formed. Stable sols exist far from this pH value. As the magnetite surface becomes negatively charged due to HA loading, its IEP is shifted to lower pHs. As a consequence, HA-coated magnetite particles form stable colloidal dispersions in a wide range of pH and salt tolerance is enhanced. In the acidic region, systems become highly unstable due to heterocoagulation.

Buckminsterfullerene C60 is an example of carbon-containing materials with diversity of potential applications, but also of unwanted environmental and health effects. Poor solubility of C60 in natural waters is a major factor controlling environmental transport and biological interactions. Adsorption of HA on buckminsterfullerene of different origin is driven by hydrophobic interactions characterized by high adsorption constants depending on the C60 and HA nature. Reported values are on the same order observed for HA and polycyclic aromatic hydrocarbons [10, 11]. The hydrophobic interaction between fullerene C60 and HA is weakened at low pH, resulting in a decrease of the binding constants.

Moreover, soil humic substances were reported to stabilize multi-walled carbon nanotube (CNT) dispersions due to the surfactant nature of HS [12]. Experiments dispersing CNT in solutions of dissolved Aldrich HA and water-extractable Catlin soil HS demonstrated enhanced stability at 150 and 300 mg/L, respectively, and decreased CNT mean particle diameter and dispersion (250 nm and 0.3 for Aldrich HA and 450 nm and 0.35 for Catlin HS, respectively). Analogous trends were observed with addition of the synthetic surfactants Brij 35, Triton X-405, and SDS. Accordingly, HA affects the deposition kinetics of hydrophobic materials as in the case of fullerene nanoparticles (C60) onto silica surfaces. In fact, C60 adsorption on bare and HA and alginate pre-coated silica surfaces was investigated over a range of monovalent (NaCl) and divalent ($CaCl_2$) salt concentrations [13]. Aggregation of fullerene nanoparticles occurs at high electrolyte concentrations.

Moreover, deposition of C60 on bare silica is controlled by electrostatic interactions and van der Waals attractions, consistent with the classical particle deposition behavior. The presence of dissolved HA and alginate leads to significantly slower deposition kinetics, as also observed by pre-coating the silica surfaces with HA and alginate in the presence of NaCl. On the other hand, even at relatively low (0.3 mM) $CaCl_2$ concentration, the deposition kinetics of fullerene nanoparticles onto both humic acid- and alginate-coated surfaces is increased. Such behavior was attributed to HA molecules undergoing complex formation with calcium ions which reduce the charge and steric influences of the adsorbed macromolecular layers.

4.3 HS-Containing Nanomaterials as Metal Scavengers

On the other hand, HS may have an important effect on the environmental uses of nanomaterials as metal scavengers. Nowadays, nanomaterials have been widely used to remove heavy metals from water/wastewater due to their large surface area and high reactivity. Since HS exist ubiquitously in aquatic environments and, as discussed before, because of their variety of functional groups, they may complex with metal ions and may be adsorbed on nanomaterials. These interactions not only alter the environmental behavior of nanomaterials, but also influence the removal and transportation of heavy metals [14]. The effects of HS on the removal and environmental behavior of heavy metal ions by nanomaterials depend on material type, pH, ionic strength, coexistence of other substances, and on the involvement of mechanisms as complex formation, adsorption, electrostatic force, oxidation/reduction, catalysis, etc. In particular, humic and fulvic acids (HA and FA, respectively) have been reported to affect the removal and mobility of heavy metals by various nanomaterials and thereby potentially alter the fate, transportation and bioavailability of heavy metals in the environment. HA/FA may change the surface properties, aggregation, transportation and toxicity of nanomaterials, and may bind metal ions by forming complexes on the mineral surface or in solution. For example, when HA and arsenic are incubated together or introduced sequentially with hematite, HA greatly reduced the sorption extent of both As(III) and As(VI) on hematite due to arsenic ions complex formation with HA. Thus, HA may promote mobility of arsenic in the environment. Generally, HA/FA influences metal bioavailability by decreasing the amount of metal ion available for the biotic ligand [14].

Liu and coauthors took advantage on HS efficiency for removing metals and developed HA-coated Fe_3O_4 nanoparticles (HA/Fe_3O_4 ~11 % w/w) for the removal of toxic Hg(II), Pb(II), Cd(II), and Cu(II) from water [15]. HA/Fe_3O_4 composites showed ~10 nm Fe_3O_4 cores and formed aggregates with average hydrodynamic size of ~140 nm. Such particle suspensions were observed to be stable in tap water, natural water, and acidic/basic solutions in the range from 0.1 M HCl to 2 M NaOH. Moreover, HA/Fe_3O_4 showed saturation magnetization

of 79.6 emu/g which allows the magnetic separation of the particles from water with low magnetic field gradients within a few minutes. Sorption of the heavy metals to HA/Fe_3O_4 reached equilibrium in less than 15 min, and could be well fitted to the Langmuir isotherm model yielding maximum adsorption capacities of 46.3–97.7 mg/g. Leaching back of the adsorbed heavy metals was found to be negligible.

HA are also capable of functioning as electron shuttle between cells and particles such as ferrihydrite [16]. In fact, microbial reduction of Fe(III) minerals at neutral pH is faced by the problem of electron transfer from the cells to the solid-phase electron acceptor. However, it was shown that Pahokee Peat HA in the presence and absence of phosphate influences the rates of Fe(III) reduction by *Shewanella oneidensis* MR-1 and the structure of the minerals formed. In general, phosphate decreases the reduction rates by sorption to the ferrihydrite thus blocking the surface sites. Addition of HA to 5 mM ferrihydrite solutions helped to overcome this inhibiting effect due to HA electron shuttling capacity. In contrast, at higher ferrihydrite concentrations (30 mM), the addition of HA leads to a decrease in the reduction rates due to ferrihydrite aggregation. In the presence of phosphate the stimulation effect occurs until a minimum concentration (10 mg/l) of dissolved HA is reached. Above dissolved HA concentrations of approximately 240 mg/l the electron shuttling effect ceased. In the presence of HA, the reduced Fe(III) mineral products yield magnetite materials of low crystallinity and smaller grain size.

4.4 HS as Reactants for the Production of Nanomaterials

HS are used as reactants for the production of nanomaterials. Silver nanoparticles (AgNP) were synthetized in Ag^+–FA solutions under relevant environmental conditions (temperature, pH, and UV light) [6]. An increase in temperature from 24 to 90 °C and pH from 6.1 to 9.0 of Ag^+–Suwannee River FA solutions accelerated the appearance of the characteristic surface plasmon resonance of AgNPs. The rate of AgNP formation via reduction of Ag^+ depended on the FA origin, which was found to be related to the FA content of free radicals. The same order of AgNP growth was seen upon UV light illumination of Ag^+–FA and Ag^+–HA mixtures in moderately hard reconstituted water. The AgNP formed were observed to be stable for several months. Transmission electron microscopy and dynamic light scattering measurements revealed bimodal particle size distributions of aged AgNP. Particles formed by fulvic and humic acid fractions of natural organic matter in the environment may be transported over significant distances and might also influence the overall bioavailability and ecotoxicity of AgNPs.

Organic–inorganic hybrid materials represent a creative alternative to design new materials and compounds with improved or unusual features which allow the development of innovative applications. Most of the hybrid materials that have already entered the market are synthesized and processed by using conventional

soft chemistry based routes [17] based on the copolymerisation of functional organosilanes, macromonomers, and metal alkoxides, the encapsulation of organic components within sol-gel derived silica or metallic oxides, and the organic functionalization of nanofillers, nanoclays, etc. Moreover, the organic template stabilizes the microscopic structure of the material upon heat-drying; thus providing a potential solution to the problem of structural changes inherent to sol-gel materials long after the completion of their synthesis. In particular, organic–inorganic hybrid materials involving natural materials offer remarkable hydrodynamic, aerodynamic, wetting, and adhesive properties [18].

4.5 Bioorganic Substances for the Synthesis of New Materials

Urban bio-wastes (UBW) have been shown to be a potential cost-effective renewable source of soluble humic-like substances known as bioorganic substances (SBO) [19]. SBO produced in relatively large scale by alkaline hydrolysis of UBW sampled from various process streams show promise as chemical auxiliaries for a number of technological applications in the chemical industry and in environmental remediation [2, 3]. UBW-SBO are mixtures of substances with molecular weights in the range (1–3) $\times$ 10^5 Da, formed by long aliphatic C chains substituted by aromatic rings and COOH, NCO, C=O, PhOH, O-alkyl, O-aryl, OCO, OMe, and alkyl amines functional groups. They have been suggested as an interesting source of biosurfactants with diversified properties depending on the nature of the waste and of its treatment process. Performance as classic surfactants and as dispersants was suggested due to their capacity to yield micelles and content of macromolecules, respectively [3]. In that sense, they were tested as a dispersant of dyes in fabric dying and as detergents for fabric cleaning. Moreover, SBO have been reported to show photosensitizing behavior as a consequence of the photoproduction of reactive radicals and excited species [20, 21] and have shown capacity as complexing agents of Fe(II/III) to drive photo-Fenton processes under non acidic conditions [22]. Because of these properties, the use of SBO in materials chemistry is wide and promising. As will be described further, they were used as templates in the synthesis of nanomaterials to yield hydrophilic surfaces, as coatings of magnetite nanoparticles for metal extraction, as templating agent-binder of mesoporous silica, TiO_2 and perovskite to be removed by calcination, and as immobilized catalyst over silica for waste water treatment.

Measurements of the SBO hydrodynamic diameter in solution indicated the formation of 130–300 nm size aggregates with no significant dependence on concentration and origin for SBO < 10 g L^{-1}. High hydrodynamic diameter values were suggested to be consistent with the macromolecular nature of these substances, in agreement with molecular weight data. Hints of the formation of large aggregates by intermolecular interactions may be found at 50–100 g L^{-1} SBO concentrations. Under these conditions SBO are no longer soluble in water

yielding rather compact viscous gel-like phases separating from the bulk water phase. Interestingly, chemical analyses indicated similar chemical composition of the organic matter in the gel phase and in the remaining aqueous phase. Whereas at concentrations <10 g L^{-1} SBO perform similarly to molecule surfactants, at concentrations >50 g L^{-1} they behave like polyelectrolytes [23].

SBO sol-gel phases can hold relatively heavy objects which laid over the gel surface with no appreciable sinking. In fact, SBO have also been reported [24] to be efficient in the flocculation of alumina, zirconia and barium titanate. Addition of 25–50 ppm SBO on 3 % alumina, zirconia and barium titanate suspensions leads to particles settling within 5 h, leaving a clear supernatant. Zeta potential measurements performed with zirconia in the presence of SBO indicates that the zero charge point is shifted from pH 8 to around pH 6.6 as a consequence of the strong interaction between the zirconia surface and the biosurfactant. Also, the surface charge was reduced significantly in the presence of the biosurfactants at all pH values. The reduction in charge was suggested to be the reason for the strong flocculation tendency of the various types of oxides studied.

The capacity of SBO to yield molecular aggregates of variable conformation and size in solution offered scope for investigating the use of SBO as templates for tailoring the morphology of inorganic oxides of use in various technological applications as catalysts, membranes, sensors and nano-electronics. SBO have been found [24] to perform as template for fabricating silica powders with 4–40 nm pore size. Silica synthesized by sol-gel reaction in the presence of the SBO showed morphology depending on the SBO concentration. In fact, silica synthesized in the absence of SBO showed few small mesopores possessing width of about 3 and 4 nm while the use of 3 g L^{-1} SBO led to a sharp pore distribution characterized by a mean pore size of 4 nm. Use of 10 g L^{-1} SBO as template led to a silica material with broad porous covering the 10–100 nm range and centered at about 30–40 nm. The differences in pore size depending on concentration are consistent with the concentration-dependent conformational changes of SBO in solution (vide supra).

(a) *Paramagnetic iron-containing hydroxyapatite nanoparticles*

The use of Ca^{2+} complexes of SBO-substrates from urban wastes as synthesis precursors of paramagnetic iron-containing hydroxyapatite nanoparticles (SBO-FeHAp) lead to significant changes in the particles morphology and surface chemistry. Among the observed effects are: a reduction of the crystallinity of hydroxyapatite domains, elongated and smaller particles with higher specific surface area, reduced Ca^{2+} content, formation of surface phosphated iron and iron oxides, increased oxygen content at the surface, and an overall negative surface charge at pH 7.0. Figure 4.1 shows the HRTEM images of pure hydroxyapatite and SBO-FeHAp nanoparticles for comparison purposes.

Moreover, formation of magnetite seems responsible for the particle paramagnetism. Such surface and structural modifications support the formation of stable homogeneous aqueous suspensions of the particles, which show a reduction of the size of the agglomerates when increasing the SBO content in the synthesis procedure.

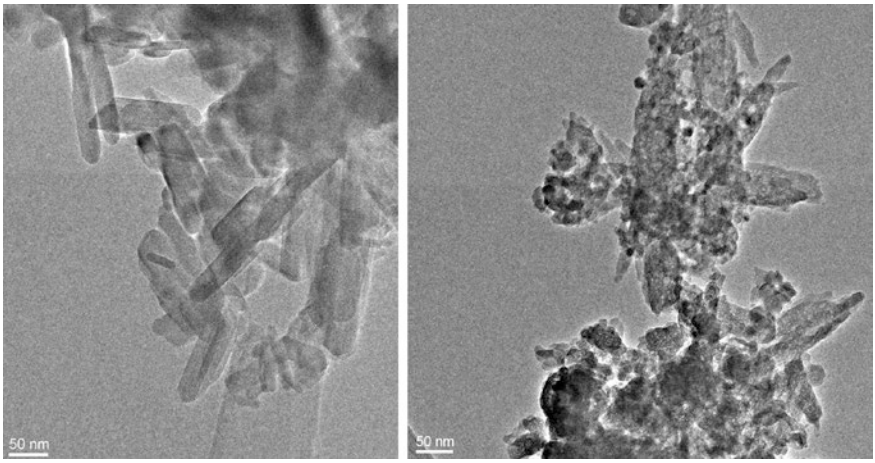

Fig. 4.1 HRTEM micrographs of pure hydroxyapatite nanoparticles (*left*) and SBO-templated paramagnetic iron-containing hydroxyapatite nanoparticles (*right*)

Testing of the SBO-templated particles as Cu^{2+} ions scavengers from aqueous solutions, indicates a significant improvement in the Cu^{2+} adsorption capacity. Maximum sorption values of 550–850 mg Cu^{2+} per gram of particles suspended in an aqueous solution at pH 7 were obtained, almost 10 times the maximum values observed for pure hydroxyapatite nanoparticles suspensions under the same conditions [18]. Such improvement is correlated with a negatively-charged surface, the presence of phosphate and Fe-OH surface groups. However, a second important effect appears to be the agglomerates size, as agglomeration seems to severely reduce the effective surface available for adsorption in aqueous suspensions. Undoubtly, these materials are a potential, self-sustaining, environmentally friendly, and efficient material for Cu^{2+} removal and aqueous effluent remediation [18]. Figure 4.2 shows a schematic diagram of the potential practical applications of the particles.

(b) *SBO-functionalized magnetic nanoparticles*

HA-stabilized magnetite nanoparticles were synthesized for their use as dyes adsorbents [25]. Considering the large similarity between humic substances and SBO, an analogous procedure was employed to prepare SBO-functionalized magnetic nanoparticles [26], as explained in Fig. 4.3. Sample, namely Fe_3O_4-SBO, can be prepared adding a black solution of SBO to an alkaline solution of Fe^{2+}/Fe^{3+} precursors, forming almost spherical particles of about 10–15 nm diameter covered by an amorphous organic phase.

The supernatant solution is quite clear at the end of the synthesis, indicating that almost all the black organic matter added is bonded to the formed particles. The solid materials can be easily separated from the synthesis medium by means of a magnetic filtration. The analysis of the interference fringe patterns and of XRD reflections confirms the presence of nanometric magnetite particles.

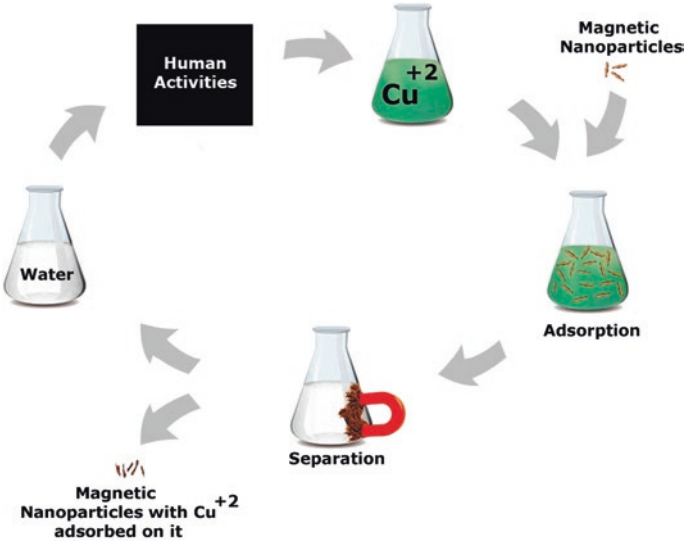

Fig. 4.2 Convenient use of magnetic HAp nanoparticles for Cu^{2+} sorption

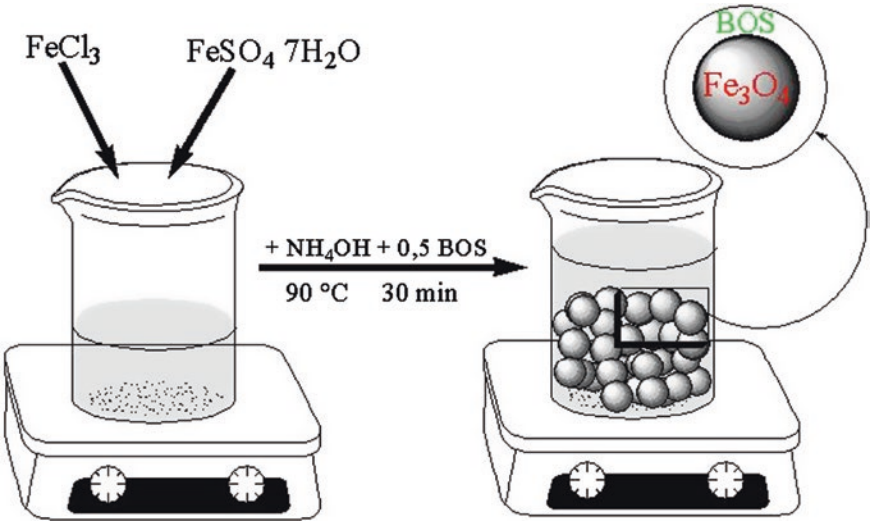

Fig. 4.3 Schematic representation of Fe_3O_4-SBO synthesis

The particles aggregation, the saturation magnetization, and the adsorbing properties were shown to be a function of SBO loading, as shown in Fig. 4.4. The adsorbing capacity was tested using two cationic dyes differing in an aminic group: Crystal violet (CV) and Malachite green (MG).

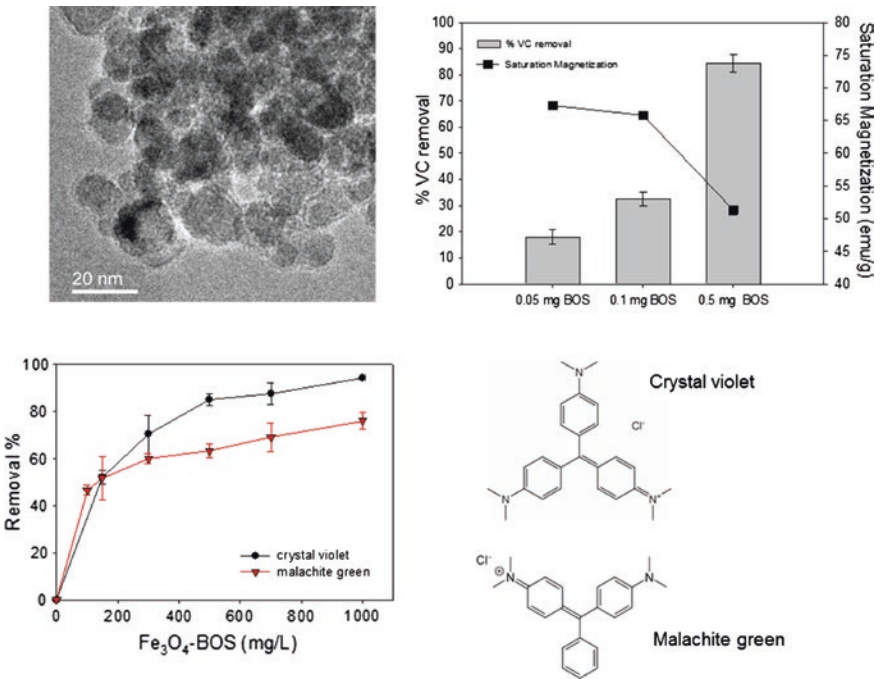

Fig. 4.4 Fe_3O_4-SBO (0.5 mg of BOS) TEM image (*top*, *left*), CV removal and saturation magnetization versus SBO loading (*top*, *right*), dyes adsorption isotherms and structure formulae of CV and MG

The adsorption isotherms evidenced promising results and the concrete possibility of using the system for dyes (organics) removal from aqueous solution. Moreover, preliminary tests, see Fig. 4.5, carried out irradiating SBO nanoparticles suspended in CV aqueous solution (Hg source, filter 300 nm) indicate a photoactivity of the system with a slow but consistent abatement of the dye. The shape of the curve and experiments carried out in the dark/light suggest that the degradation reaction occurs after a preliminary adsorption step.

(c) *SBO functionalized silica*

SBO was covalently immobilized on the surface of amorphous silicas with different morphology activated with aminopropyl groups and using 1-ethyl-3-(3-dimethylaminopropyl)carbodiimide (EDC) in one-pot procedure with SBO molecules following a protocol developed by Silva et al. [27] and extended to SBO grafting by Testa et al. [28]. The materials contained ~34 % w/w of organic matter were tested in order to verify the photoactivity of SBO molecules after their chemical immobilization on siliceous supports. The aim of this procedure is to obtain a heterogeneous photocatalyst active in pollutants abatement.

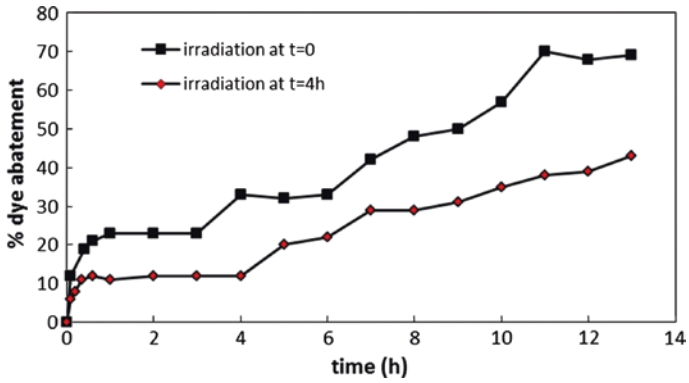

Fig. 4.5 VC degradation followed by UV-Vis spectroscopy at 583 nm. *Black points:* experiment with light irradiation at t = 0. *Red points:* experiment with a preliminary adsorption step carried out in the dark for 4 h before light irradiation

The morphologic characterization of powders are summarized in Table 4.1.

The data in Table 4.1 clearly suggest that the functionalization procedure greatly affects the morphologic behavior of the starting silicas, in particular dealing with HMS sample: the specific surface area decreases as well as the total mesoporosity. Nevertheless, preliminary irradiation experiments results obtained using 4-methylphenol as substrate in a solarbox (Xe lamp, filter 340 nm), indicate a good activity of all the functionalized silicas towards 4-methylphenol abatement versus a negligible substrate adsorption. Overall, the results suggest that the activity of the materials is not only due to the contact between powders and substrate but also to reactive species produced by SBO molecules (Fig. 4.6).

The same test (methylphenol abatement in Solarbox) was carried out grafting deashed SBO (i.e., treated in order to eliminate the inorganic residues) on the amorphous silica: in this case the abatement improves by *ca* 10 %, indicating that the removal of inorganic residues is beneficial for sample photoactivity.

Table 4.1 Surface area and total mesoporosity determined from N_2 adsorption curves at 77 K fitted to BET isotherms

Samples	BET (m^2/g)	BJH total mesoporosity (cm^3/g)
Amorphous SiO_2	514	1.73
Amorphous SiO_2 + SBO	137	0.07
Amorphous SiO_2 + deashed SBO	65	0.15
BA	755	2.40
SBA + SBO	79	0.14
HMS	997	1.51
HMS + SBO	5	Not measurable

SBA stands for SBA-15, HMS corresponds to hexagonal mesoporous silica

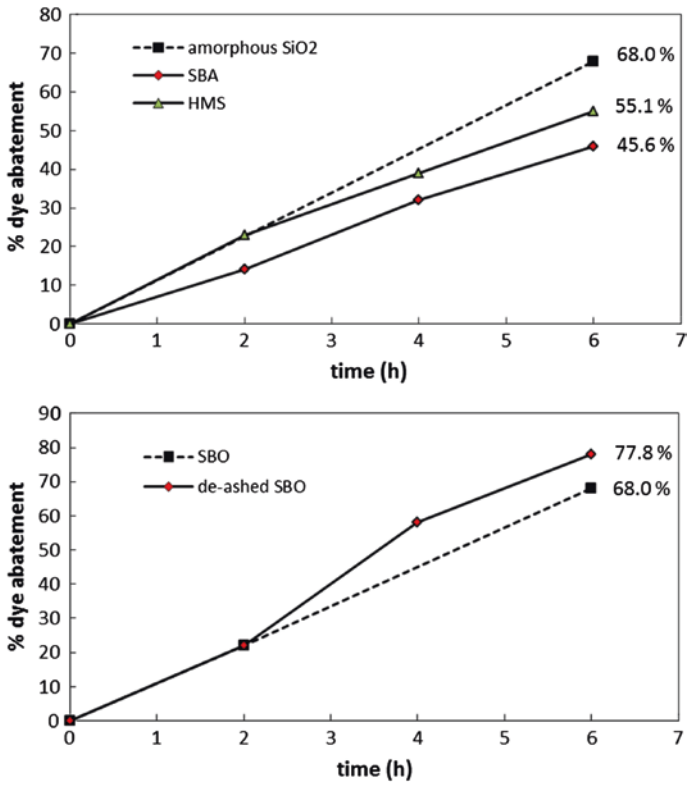

Fig. 4.6 Abatement of 10 ppm of 4-methylphenol after irradiation in a solarbox (Xenon lamp, 1,500 W, filter at 340 nm) in the presence of 1,200 ppm SBO-functionalized silica (*top*) and amorphous silica functionalized with SBO (as is and deashed, *bottom*)

(d) *Mesoporous siliceous monoliths*

Mesoporous siliceous monoliths were prepared by using commercial silica nanoparticles and SBO as templating agent-binder to be removed by calcination at 450 °C [29]. The heterogeneous nature of SBO, which is composed by organic matter with surfactant properties and by inorganic residues (alkaline and hearth-alkaline salts, among others, and silica), allows to obtain handlable aggregates of silica particles fused together (with the inorganic residues acting as glass frit bonding components [30]) with mesoporosity brought about by surfactant molecules aggregation and micellization (Fig. 4.7).

Monoliths were prepared starting from two different commercial silicas, one pyrogenic and essentially hydrophobic (namely, A300 by Degussa), and one prepared via precipitation in water and hydrophilic (namely, Sipernat 320 by Evonik). Aim of the work was thought in the field of water remediation and was twofold: (i) to prepare mesoporous siliceous monoliths with modulated hydrophilicity/hydrophobicity

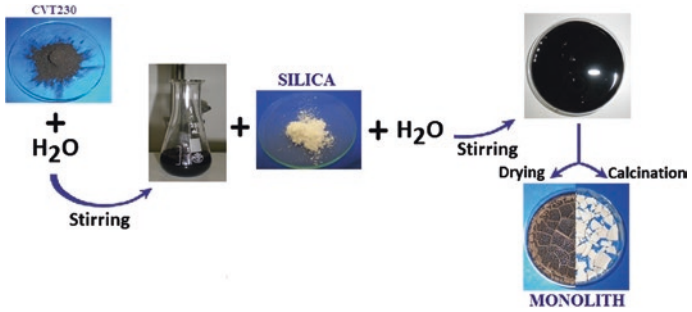

Fig. 4.7 Schematic representation of monolith production, From *left* to *right* SBO stirred in water, addition of silica powder to the mixture, suspension put in a Pyrex Petri dish for drying and following calcination in oven at 450 °C for 3 h. The *last bottom figure* represent the monolith before and after the calcination treatment

(considering various mixtures of the two starting silicas) to be used as adsorbing materials towards hydrophilic or hydrophobic pollutants, and (ii) to prepare biocatalytic handlable devices by means of enzyme covalent immobilization for pollutant degradation.

Considering the latter application, the mesoporous monoliths were surface functionalized using Soybean Peroxidase (SBP) [29] and Lipase from *Candida antarctica* [31]. In both cases the enzymes were immobilized on aminopropyl-functionalized monoliths using glutaraldehyde molecules as spacers (Fig. 4.8).

The covalent immobilization of SBP on hydrophobic A300-based monolith failed, as indicated by experimental results carried out with DMAB/MBTH (at pH = 5.4 in the presence of H_2O_2). SBP activates H_2O_2 molecules allowing the formation of a violet compound observable via UV-VIS spectroscopy at 590 nm. The first reaction cycle occurs with a very limited reaction yield which decreases

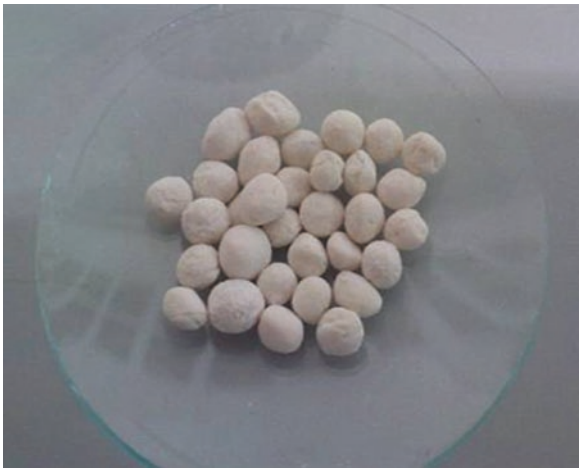

Fig. 4.8 Hand-made spheres of Sipernat 320-based SiO_2: the diameter of each sphere is approximatively 0.5 cm

to zero in the second reaction cycle, indicating that the enzyme is bonded to the A300-monolith surface only via weak physical adsorption and suggesting that the hydrophobic support is not suitable in covalently bonding SBP species.

The best results were obtained immobilizing SBP on hydrophilic Sipernat 320-based monolith: for this system an activity percentage of 100 % (measured as % decrease of absorbance at 590 nm) was reached in 3 h of reaction. Furthermore, the system is stable and retains about 80 % of its initial activity after 20 reaction cycles.

On the other hand, lipase immobilization showed opposite results. When the protein was immobilized on a Sipernat 320-based monolith, and tested with p-nitrophenyl dodecanoate (p-NPD) at pH = 7 monitoring the hydrolysis and the following formation of p-nitrophenol spectrophotometrically, the results indicate that the catalytic activity of this system is not relevant. Hydrolysis specific rate is very close to zero value, probably because the active centers of the enzyme are closed to the access of the substrate because of the hydrophilic nature of supporting monolith.

Good results were indeed obtained with p-NPD hydrolysis carried out with immobilizing lipase on hydrophobic A300-based monoliths. The reaction yield is fair and, above all, the immobilized enzyme results much more stable than free enzyme after 7 days of storing in the dark at pH = 7.5 and T = 4 °C.

The results above described indicate that the hydrophilicity/hydrophobicity degree of the support (whose properties can be modulated through the choice of the appropriate starting material) can affect both the enzyme immobilization results and the catalytic activity of the biocatalyst (i.e., favoring or prejudicing support-substrate interactions).

(e) *Perovskite material*

$LaFeO_3$ is a perovskite mixed oxide which can be used as photocatalyst activated by visible light and/or as material for fuel cell electrodes thanks to the high mobility of oxygen species present in its framework.

The oxide was synthesized by an auto-combustion method [32] using soluble bio-organic substances (SBO) extracted from composted urban wastes [19]. In this synthesis SBO replaced the traditional citric acid, as fuel, templating and chelating agents, while metal nitrates represented metal sources and oxidizers [33]. The synthesis parameters (such as pH, fuel-to-metal cations ratio and reducers-to-oxidizers ratio) were optimized and SBO isolated from waste with different behaviours were employed to test how they can affect the synthesis products. The morphologic, structural and chemical characterization of the samples was carried out by means of X-Ray Diffraction combined with Rietveld refinement, Scanning and Transmission Electron Microscopies, gas-volumetric N_2 uptake at 77 K and FTIR spectroscopy. All samples showed 5–10 m^2/g of specific surface area and limited mesoporosity, but a sonication treatment allows to largely increase these values causing the opening of closed porosities formed during the auto-combustion process [34, 35]. $LaFeO_3$ samples were used as photo-catalysts for the abatement of two model contaminants: Crystal Violet, a cationic dye, and 4-methylphenol, a representative phenolic compound that could be found in wastewaters. In the first case, pollutant abatement reached 100 % of yield at suspension pH = 9.8, whereas

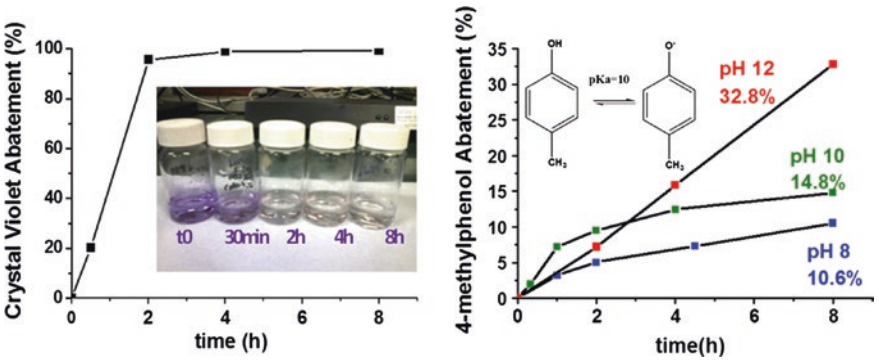

Fig. 4.9 Abatement of crystal violet (*left*) and 4-methylphenol (*right*) with $LaFeO_3$. Experiments performed with 10 mg/L of substrate and 1,200 mg/L of photocatalyst in solarbox, with xenon lamp and cut-off filter for wavelengths below 340 nm

the photo-degradation of 4-methylphenol was less efficient and greatly influenced by pH, with abatment yield from 10 % at pH = 8 up to 33 % at pH = 12. The analysis of the ζ potential of the particles versus pH indicates that the different reactivity is influenced by the different charge of the material surface and by the subsequent approach of the substrates to the photocatalyst surface (Fig. 4.9).

(f) *Mesoporous TiO_2*

Mesoporous TiO_2 was synthesized via sol-gel procedure using BOS as templating/structure-directing agent and characterized by means of physico-chemical techniques (TEM, XRD, adsorption of N_2 at 77 K, water adsorption microcalorimetry) [36]. The aim of the work was to produce a high surface mesoporous photocatalysts, but the characterization results opened the way to further considerations concerning SBO properties.

The TEM images and the relevant characterization data relative to TiO_2 materials are reported in Fig. 4.10 and Table 4.2.

The analysis of the particle size evidenced by TEM images and calculated by Scherrer equation from XRD signals indicates that SBO molecules affect the TiO_2 particles formation and growth, since, as demonstrated in the literature for yeast templated TiO_2 material [37], ionic moieties in the SBO molecules can behave like nucleation sites towards ionic oxide formation. The gel formed in the presence of high SBO concentration (sample TiO_2-SBO50) is OH-reach with respect to the non-templated one, giving an oxide with hydrophilic surface and extensive aggregation of the primary particles. The latter property reflects on N_2 adsorption data which show the decrease of the apparent specific surface area and of interparticle porosity increasing SBO amount in synthesis procedure.

The comparison of the results obtained for TiO_2 and SiO_2 prepared in the presence of SBO [24] indicates that the biosurfactant plays a different role when used in the presence of TEOS (tetraethyl orthosilicate, SiO_2 precursor) and TIIP

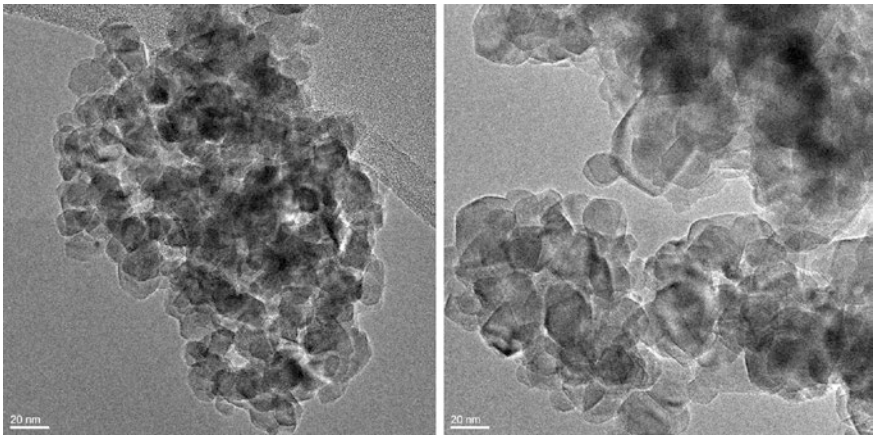

Fig. 4.10 TEM images relative to TiO_2 (*left*) and TiO_2-SBO50 (*right*) samples

Table 4.2 Morphological and structural features of TiO_2 samples as obtained from XRD and gas-volumetric adsorption of N_2 at 77 K

Samples	XRD results		N_2 adsorption at 77 K		
	Crystalline phases	Particle size from Scherrer (nm)	Specific surface area (m^2/g)	Larger pore size from BJH (nm)	Pore volume from BJH (cm^3/g)
TiO_2	Anatase + brookite	18	88	21	0.45
TiO_2-SBO10	Anatase	11	80	10	0.30
TiO_2-SBO50	Anatase	10	69	7	0.19

(Titanium tetraisopropoxide, TiO_2 precursor). In the first case SBO molecules act as real templating agents forming silica with increasing porosity upon increasing SBO amount in synthesis procedure. In the latter case SBO molecules interact with Ti^{4+} species forming a large number of nucleation sites during TiO_2 formation, increasing the hydrophilicity and the aggregation of the oxide particles and limiting, at the same time, their growth.

References

1. Dudare, D., & Klavins, M. (2013). Peat humic substances as sorbent for nanomaterials. In *13th SGEM GeoConference on Nano, Bio and Green-Technologies for a Sustainable Future* (pp. 67–74.). www.sgem.org, SGEM2013 Conference Proceedings. ISBN 978-619-7105-06-3/ISSN 1314-2704.
2. Montoneri, E., Boffa, V., Quagliotto, P. L., Mendich, R., Chierotti, M. R., Gobetto, R., & Medana, C. (2008). Humic acid-like matter isolated from green urban wastes. Part I: Structure and surfactant properties. *BioResources, 3*, 123–141.

3. Montoneri, E., Savarino, P., Bottigliengo, S., Musso, G., Boffa, V., Bianco Prevot, A., et al. (2008). Humic acid-like matter isolated from green urban wastes. Part II: Performance in chemical and environmental technologies. *BioResources, 3*, 217–233.
4. Gu, B., Schmitt, J., Chen, Z., Liang, L., & McCarthy, J. F. (1994). Adsorption and desorption of natural organic matter on iron oxide: Mechanisms and models. *Environmental Science and Technology, 28*, 38–46.
5. Zhang, Y., Chen, Y., Westerhoff, P., & Crittenden, J. (2009). Impact of natural organic matter and divalent cations on the stability of aqueous nanoparticles. *Water Research, 43*, 4249–4257.
6. Adegboyega, N. F., Sharma, V. K., Siskova, K., Zbořil, R., Sohn, M., & Schultz, B. J. (2013). Interactions of aqueous Ag^{+} with fulvic acids: mechanisms of silver nanoparticle formation and investigation of stability. *Environmental Science and Technology, 47*, 757–764.
7. Yang, K., Lin, D., & Xing, B. (2009). Interactions of humic acid with nanosized inorganic oxides. *Langmuir, 25*, 3571–3576.
8. Ohashi, H., & Nakazawa, H. (1996). The microstructure of humic acid montmorillonite composites. *Clay Minerals, 31*, 347–354.
9. Illés, E., & Tombácz, E. (2006). The effect of humic acid adsorption on pH-dependent surface charging and aggregation of magnetite nanoparticles. *Journal of Colloid and Interface Science, 295*, 115–123.
10. Maris, K., & Linda, A. (2009). Study of interaction between humic acids and fullerene C60 using fluorescence quenching approach. *Ecological Chemistry and Engineering S, 17*, 351–362.
11. Klavins, M., Ansone, L., & Zicmanis, A. (2011). Behaviour of nanomaterials in the environment: A study of interaction between humic acids and fullerene C60. *Latvian Journal of Chemistry, 49*, 283–293.
12. Chappell, M. A., George, A. J., Dontsova, K. M., Porter, B. E., Price, C. L., Zhou, P., et al. (2009). Surfactive stabilization of multi-walled carbon nanotube dispersions with dissolved humic substances. *Environmental Pollution, 157*, 1081–1087.
13. Chen, K., & Elimelech, M. (2008). Interaction of fullerene (C60) nanoparticles with humic acid and alginate coated silica surfaces: Measurements, mechanisms, and environmental implications. *Environmental Science and Technology, 42*, 7607–7614.
14. Tang, W.-W., Zeng, G.-M., Gong, J.-L., Liang, J., Xu, P., Zhang, C., & Huang, B.-B. (2014). Impact of humic/fulvic acid on the removal of heavy metals from aqueous solutions using nanomaterials: A review. *Science of the Total Environment, 468–469*, 1014–1027.
15. Liu, J.-F., Zhao, Z.-S., & Jiang, G.-B. (2008). Coating Fe_3O_4 Magnetic nanoparticles with humic acid for high efficient removal of heavy metals in water. *Environmental Science and Technology, 42*, 6949–6954.
16. Amstaetter, K., Borch, T., & Kappler, A. (2012). Influence of humic acid imposed changes of ferrihydrite aggregation on microbial Fe(III) reduction. *Geochimica et Cosmochimica Acta, 85*, 326–341.
17. Sanchez, C., Julian, B., Belleville, P., & Popall, M. (2005). Applications of hybrid organic–inorganic nanocomposites. *Journal of Materials Chemistry, 15*, 3559–3592.
18. Mercado, D. F., Magnacca, G., Malandrino, M., Rubert, A., Montoneri, E., Celi, L., et al. (2014). Paramagnetic iron-doped hydroxyapatite nanoparticles with improved metal sorption properties. A Bio-organic substrates-mediated synthesis. *ACS Applied Materials and Interface, 6*, 3937–3946.
19. Montoneri, E., Mainero, D., Boffa, V., Perrone, D. G., & Montoneri, C. (2011). Biochemenergy: a project to turn an urban wastes treatment plant into biorefinery for the production of energy, chemicals and consumer's products with friendly environmental impact. *International Journal of Global Environment Issues, 11*, 170–196.
20. Bianco Prevot, A., Fabbri, D., Pramauro, E., Baiocchi, C., Medana, C., Montoneri, E., & Boffa, V. (2010). Sensitizing effect of bio-based chemicals from urban wastes on the photodegradation of azo-dyes. *Journal of Photochemistry and Photobiology A: Chemistry, 209*, 224–231.

21. Bianco Prevot, A., Avetta, P., Fabbri, D., Laurenti, E., Marchis, T., Perrone, D. G., et al. (2011). Waste derived bioorganic substances for light induced generation of reactive oxygenated species. *ChemSusChem, 4*, 85–90.
22. Gomis, J., Vercher, R. F., Amat, A. M., Mártire, D. O., González, M. C., Bianco Prevot, A., et al. (2013). Application of soluble bio-organic substances (SBO) as photocatalysts for wastewater treatment: Sensitizing effect and photo-Fenton-like process. *Catalysis Today, 209*, 176–180.
23. Montoneri, E., Boffa, V., Savarino, P., Perrone, D. G., Montoneri, C., Mendichi, R., et al. (2010). Behaviour and properties in aqueous solution of bio-polymers isolated from urban refuse. *Biomacromolecules, 11*, 3036–3042.
24. Boffa, V., Perrone, D. G., Montoneri, E., Magnacca, G., Bertinetti, L., Garlasco, L., & Mendichi, R. (2010). A waste derived biosurfactant for preparation of templated silica powders. *ChemSusChem, 3*, 445–452.
25. Carlos, L., Cipollone, M., Soria, D. B., Sergio Moreno, M., Ogilby, P. R., García Einschlag, F. S., & Mártire, D. O. (2012). The effect of humic acid binding to magnetite nanoparticles on the photogeneration of reactive oxygen species. *Separation and Purification Technology, 91*, 23–29.
26. Magnacca, G., Allera, A., Montoneri, E., Celi, L., Benito, D. E., Gagliardi, L. G., et al. (2014). *ACS Sustainable Chemistry & Engineering, 2*, 1518–1524.
27. Silva, A. R., Wilson, K., Clark, J. H., & Freire, C. (2006). Covalent attachment of chiral manganese(III) salen complexes onto functionalised hexagonal mesoporous silica and application to the asymmetric epoxidation of alkenes. *Microporous and Mesoporous Materials, 91*, 128–138.
28. Testa, M. L., Tummino, M. L., Agostini, S., Avetta, P., Deganello, F., Montoneri, E., Magnacca, G., Bianco Prevot, A. Synthesis, characterization and environmental application of silicas modified with waste-derived photoactive substances. Submitted to *Chemical Engineering Journal*.
29. Magnacca, G., Laurenti, E., Vigna, E., Franzoso, F., Tomasso, L., Montoneri, E., & Boffa, V. (2012). Refuse derived bio-organics and immobilizer soybean peroxidase for green chemical technology. *Process Biochemistry, 47*, 2025–2031.
30. Knechtel, R. (2005). Glass frit bonding: an universal technology for wafer level encapsulation and packaging. *Microsystem Technologies, 12*, 63–68.
31. Lupasteanu, A. M., Laurenti, E., Magnacca, G., & Montoneri, E. (2012). New monolith configuration for the immobilization of lipase from *Candida antarctica*. *Environment Engineering and Management Journal, 11*, 2023–2028.
32. Deganello, F., Marcì, G., & Deganello, G. (2009). Citrate–nitrate auto-combustion synthesis of perovskite-type nanopowders: A systematic approach. *Journal of the European Ceramic Society, 29*, 439–450.
33. Deganello, F., Tummino, M. L., Calabrese, C., Testa, M. L., Avetta, P., Fabbri, D., Bianco Prevot, A., Montoneri, E., Magnacca, G. (2014). New eco-friendly $LaFeO_3$ material prepared from urban wastes New *Journal of Chemistry*, *2014*. doi:10.1039/C4NJ01279H.
34. Magnacca, G., Spezzati, G., Deganello, F., & Testa, M. L. (2013). A new in situ methodology for the quantification of the oxygen storage potential in perovskite-type materials. *RSC Advances, 3*, 26352–26360.
35. Jabariyan, S., & Zanjanchi, M. A. (2012). A simple and fast sonication procedure to remove surfactant templates from mesoporous MCM-41. *Ultrasonics Sonochemistry, 19*, 1087–1093.
36. Boffa, V., Perrone, D. G., Magnacca, G., & Montoneri, E. (2014). Role of a waste-derived biosurfactant in the sol-gel synthesis of nanocrystalline titanium dioxide. *Ceramic International, 40*, 12161–12169.
37. He, W., Cui, J., Yue, Y., Zhang, X., Xia, X., Liu, H., & Lui, S. (2011). High-performance TiO_2 from Baker's yeast. *Journal of Colloid and Interface Science, 354*, 109–115.

Chapter 5
Mathematical Modeling for SBO Applications

A.C.S.C. Teixeira, A.M. Lastre Acosta, A.S. Vianna Jr and G.A.C. Le Roux

Abstract Modeling and simulation are recognized as extremely valuable tools for developing new materials by increasing efficiently the knowledge on systems. The mathematical tools and methods necessary to build a wide range of models are presented here. Two case studies illustrate the different mathematical approaches introduced: the SDZ photodegradation in SBO and the adsorption in SBO-magnetite particles.

Keywords SBO · Modeling · Simulation · Parameter estimation · Photo-Fenton · Photodegradation · Adsorption

5.1 Introduction

There is great variety of books and references that introduce mathematical modeling for a wide range of different systems. In this chapter we would not dare to be as ambitious as to give a new contribution to this traditional theme. Two interesting applications involving SBO are presented and the theory necessary to understand the methods used in both the applications is rapidly presented. A list of references that can be useful in dealing with new problems is presented.

A.C.S.C. Teixeira (✉) · A.M. Lastre Acosta · A.S. Vianna Jr · G.A.C. Le Roux
Department of Chemical Engineering, University of São Paulo, Av. Prof. Luciano Gualberto Trav. 3, 380, 05508-010 São Paulo, SP, Brazil
e-mail: acscteix@usp.br

A.M. Lastre Acosta
e-mail: arlenlastre@gmail.com

A.S. Vianna Jr
e-mail: ardson@usp.br

G.A.C. Le Roux
e-mail: galoroux@usp.br

A. Arques and A. Bianco Prevot (eds.), *Soluble Bio-based Substances Isolated From Urban Wastes*, SpringerBriefs in Green Chemistry for Sustainability,
DOI 10.1007/978-3-319-14744-4_5

A mathematical model is a collection of equations that are suited to represent the quantitative relation between variables. Roughly, variables can be classified into three different groups:

- independent (noted x);
- dependent (noted **y**);
- parameters (noted **θ**).

Independent variables are variables that can be set by the experimenter, such as temperature, initial reactant concentration or catalyst concentration in a reaction, for instance. Dependent variables are variables that correspond to the result of the experiment, or in other words, that are the consequence of the experimental conditions set. These variables correspond to what is aimed to be predicted. A model can be expressed through the following mathematical notation [1]:

$$\mathbf{y} = \mathbf{f}(\mathbf{x}, \boldsymbol{\theta}) \tag{5.1}$$

5.2 Fundamentals of Model Adaptation

A model is only valuable if it represents the reality as well as needed for the objective it is suited for [2]. In other terms, the objective of adjusting a mathematical model to experimental data is to obtain a representation of the system as accurate as possible and as useful for a particular application.

In order to perform this important task many different techniques are available but the basis for model adaptation is to understand that the final model must fit the data as good as possible, without overfit. The overfit is a pathology that must be avoided because when it arises, some deterministic features of the model serve as to represent random errors, making extrapolation uncertain.

On the other hand, if the model is too simple, it will be impossible to represent some features of the phenomenon. The built of such a mathematical model is an iterative task, where models are proposed, adjusted to the experimental data and modified until the utility requirement is reached. The iterative procedure could point out also that more experimental data should be obtained in order to improve the utility of the final model.

5.2.1 Strategies

In fitting the model a criterion must be assumed that measures the distance between the model and the experimental data. Criteria are in general based on statistical assumptions, as for maximum likelihood family, but the choice is very wide. The simpler choice is the Euclidean distance, termed as the sum of the square of the difference between measured and predicted quantities [3, 4]. The estimator defined by minimizing the former criterion is the well-known least square estimator.

The problem is that if a model is too complex, in other words, if it possesses too many parameters, the criterion can get very small, but predictions accuracy would degrade and thus get much less reliable. This is what is called the overfit.

As far as the model gets more complex its potential overfit gets of great concern. There are two ways to avoid overfit: by controlling the complexity of the model (the parsimony principle, also called Ockham's razor) or by using a strategy based on prediction accuracy, whose aim is not to reach the best fit, but the best prediction capability.

5.2.1.1 Models Linear in Parameters

In what is called surface response techniques, models that are linear in parameters are used. Models linear in parameters are models in which the independent variables are postulated as the sum of the product of nonlinear parts, termed regressors, and parameters, as in Eq. 5.2:

$$\mathbf{y} = \mathbf{f}(\mathbf{x}, \boldsymbol{\theta}) = \sum_{\mathbf{i}=\mathbf{1}}^{\mathbf{p}} \boldsymbol{\theta}_\mathbf{i} \mathbf{r}_\mathbf{i}(\mathbf{x}) \tag{5.2}$$

A polynomial is a model linear in parameters, where the regressors are products of independent variables raised to integer powers. One of the great advantages of models linear in parameters is that the values of the parameters that minimize a sum of squares criterion can be obtained analytically, without any iterative procedure.

Many experimental designs that make the procedure more efficient are available in literature. The most widely used is the factorial design where combinations of the independent variables taken at their maximum and minimum are used, and are optimal for linear regressors. For second order polynomials Box-Behnken design, that makes use of the central point is mostly used, but the Doehlert design, where some independent variables are taken at intermediate values (not maximal, nor minimal, nor central) is the more efficient as less experimental points are needed in order to fit a model of second degree.

The goodness of fit is assessed by means of parity plots and correlation statistics, like R^2. After the model is adjusted, the parameters estimates are tested in order to verify if their value is significantly different from zero. If not, they are removed from the model following parsimony principle, thus serving to avoid model overfit.

Many commercial softwares perform this kind of analysis. Even most commercial spreadsheet calculators can perform some of the tasks for surface response analysis.

5.2.1.2 Models Nonlinear in Parameters

Models nonlinear in parameters cannot be expressed as in Eq. 5.2. The complexity of the problem of fitting nonlinear models is increased because the solution becomes

iterative. The solution cannot be obtained analytically, but only through an iterative algorithm like Newton-Raphson or Levemberg-Marquardt. Many numerical environments like Matlab or Scilab perform this kind of calculation.

The problem is that the convergence to a solution is not guaranteed, the existence of an unique solution cannot be proven a priori and pathologies like practical unidentifiability [5] make more difficult to diagnose if the models are overfitted, or if problems are due to numerical convergence issues, or to oversimplified models, or even to gross experimental errors.

Solutions are difficult to obtain and a good amount of know-how is still necessary in spite of the stage of development of the computational tools. The goodness of fit is assessed as for linear models, and parameters estimates are analyzed in terms of individual confidence intervals of the parameters because they are indirectly an indicator of the overfit of the model.

5.2.1.3 Overparameterized Models

In cases where models based on first principles would be too complex, extremely flexible models with an impressively large number of parameters are an alternative. Artificial Neural Networks are a great example of this kind of models but some categories of linear models, with a huge number of independent variables has also become very frequent, and made useful through Pseudo Least Squares technique.

Feed-forward Artificial Neural Networks present a very large number of parameters that can be larger than the number of experimental data. This kind of model is extremely flexible and is able to fit any phenomena, depending on the number of neurons considered.

In order to make predictions reliable the objective of obtaining parameters that make the model as close to the experimental data is left aside, instead, the capability of prediction is tested on a data set (Test Set) that is not used to adjust the model (Learning Set). Thus, parameters are only updated as far as their prediction is improved. Once the prediction in the Test Set is not improved anymore, parameters are not updated any further. This kind of approach is very good for interpolation, but extrapolation, that is, predicting in conditions outside the Learning and Test Sets domain, should be cautiously avoided.

5.3 Applications (Case Studies)

5.3.1 Application to an Advanced Oxidation Process Enhanced with SBO

Large amounts of antibiotics have been detected in different aqueous matrices throughout the world. However, some of these pharmaceutical products are not eliminated completely by conventional biological and physicochemical-based

treatments in sewage treatment plants. Among them, sulfadiazine is not readily biodegradable and has been frequently detected in drinking water, surface water, groundwater and wastewater from treatment plants [6].

Advanced oxidation processes (AOP) are highly promising for the remediation of contaminated aqueous systems; among them the photo-Fenton process has been widely used. The change of pH has significant effects on the Fenton reaction and the optimum is generally accepted to be around 3 [7]. At higher pH, the system efficiency is decreased since iron ions precipitate as iron hydroxide. This issue is a serious constraint for the employment of the photo-Fenton process in full-scale operation. Therefore, iron complexation in the presence of organic compounds seem promising for extending the optimum pH range, as reported for humic acids [8].

Soluble bio-organic substances (SBO) obtained from urban bio-wastes have been used as chemical auxiliaries in photochemical processes for environmental remediation [8–10]. They contain a significant mineral portion, in particular iron. For this reason, the photo-Fenton process might be driven with these compounds. In the following paragraphs, we briefly discuss the use of response surface technique and neural network modeling for the study of the photo-Fenton degradation of the antibiotic sulfadiazine (SDZ) in the presence of SBO CVT230 [8].

5.3.1.1 Doehlert Uniform Array Design for Three Variables and Response Surface Model

A Doehlert uniform array design was used to investigate the effects of $[Fe^{3+}]_0$ (1–15 mg L^{-1}), $[SBO]_0$ (5–50 mg L^{-1}) and pH (3, 5 and 7) on SDZ photodegradation. The experiments were carried out at $[SDZ]_0 = 25$ mg L^{-1} and $[H_2O_2]_0 = 244$ mg L^{-1}, according to Table 5.1. In this study, t_{50} (half-life time, min) was selected as the response variable.

Multiple regression analysis based on the least square method was performed using Statgraphics® Centurion XVI software. The model for t_{50} is a second-order polynomial equation with ten coefficients (Eq. 5.3) where X_1, X_2 and X_3 are the coded variables studied ($[Fe^{3+}]_0$, $[SBO]_0$ and pH, respectively). The results of the regression analysis are listed in Table 5.2. The significance of each effect was evaluated based upon the F-test with $P < 0.05$. The determination coefficient, R^2, was equal to 0.995. According to the standardized Pareto chart, within the range of values of parameters studied, the effects of pH and SBO played the most important roles on the half-life time (t_{50}, min). The marked effect of pH is expected regarding the efficiency of the Fenton reaction.

$$t_{50} = b_0 + b_1X_1 + b_2X_2 + b_3X_3 + b_{11}X_1^2 + b_{22}X_2^2 + b_{33}X_3^2 + b_{12}X_1X_2 + b_{13}X_1X_3 + b_{23}X_2X_3 \quad (5.3)$$

The effects of Fe^{3+} and SBO on t_{50} at different pH values (3, 5 and 7) are shown in the surface response contour plots (Fig. 5.1).

Table 5.1 Doehlert design matrix for three factors and experimental values of t_{50}[a]

Exp.	X_1	X_2	X_3	$[Fe^{3+}]_0$ (mg L^{-1})	$[SBO]_0$ (mg L^{-1})	pH	t_{50} (min)
1	0	0	0	8	27.5	5	46.6
1A	0	0	0	8	27.5	5	51.2
1B	0	0	0	8	27.5	5	48.8
2	1	0	0	15	27.5	5	36.7
3	0.5	0.866	0	11.5	50.0	5	40.7
4	0.5	0.289	0.817	11.5	35.0	7	109.8
5	−1	0	0	1	27.5	5	51.0
6	−0.5	−0.866	0	4.5	5.0	5	60.6
7	−0.5	−0.289	−0.817	4.5	20.0	3	5.8
8	0.5	−0.866	0	11.5	5.0	5	39.8
9	0.5	−0.289	−0.817	11.5	20.0	3	5.6
10	0	0.577	−0.817	8	42.5	3	4.4
11	−0.5	0.866	0	4.5	50.0	5	33.4
12	−0.5	0.289	0.817	4.5	35.0	7	132.1
13	0	−0.577	0.817	8	12.5	7	152.6

aVariables X_1, X_2 and X_3 represent the codified values of $[Fe^{3+}]_0$, $[SBO]_0$ and pH, respectively

Table 5.2 Model coefficients and estimated effects of the factors on t_{50} by multiple regression analysis

	Coefficients	Estimated effects
Mean	48.9 (b_o)	48.9^{***}
X_1: Fe^{3+}	−8.1 (b_1)	-16.2^{***}
X_2: SBO	−10.5 (b_2)	-18.1^{***}
X_3: pH	77.3 (b_3)	126.24^{***}
X_1^2	−5.0 (b_{11})	-10.0^{ns}
X_1 X_2	16.2 (b_{12})	28.1^{***}
X_1 X_3	−19.3 (b_{13})	-31.5^{***}
X_2^2	−5.3 (b_{22})	-8.0^{ns}
X_2 X_3	−21.5 (b_{23})	-30.5^{***}
X_3^2	31.8 (b_{33})	42.5^{***}

***Significant ($P < 0.05$), ^{ns}Non-significant

At pH 5 the region of minimum for t_{50} is expected for low and high levels of Fe^{3+} and SBO, respectively. The same situation is observed in the opposite case (low SBO and high Fe^{3+} levels). A possible explanation for this behavior is related to the fact that, when Fe^{3+} is at low concentrations, organic compounds present in the SBO would be able to complex iron cations and as a result metal precipitation would be avoided. By contrast, for Fe^{3+} at high concentrations, a large amount of SBO would not be needed for the photo-Fenton process. At pH 7, the SBO was able to enhance the photo-Fenton reaction but high levels of Fe^{3+} and SBO are needed to increase the efficiency of the process as shown in Fig. 5.1c. Contrary, at pH 3 high levels of these variables are not advisable.

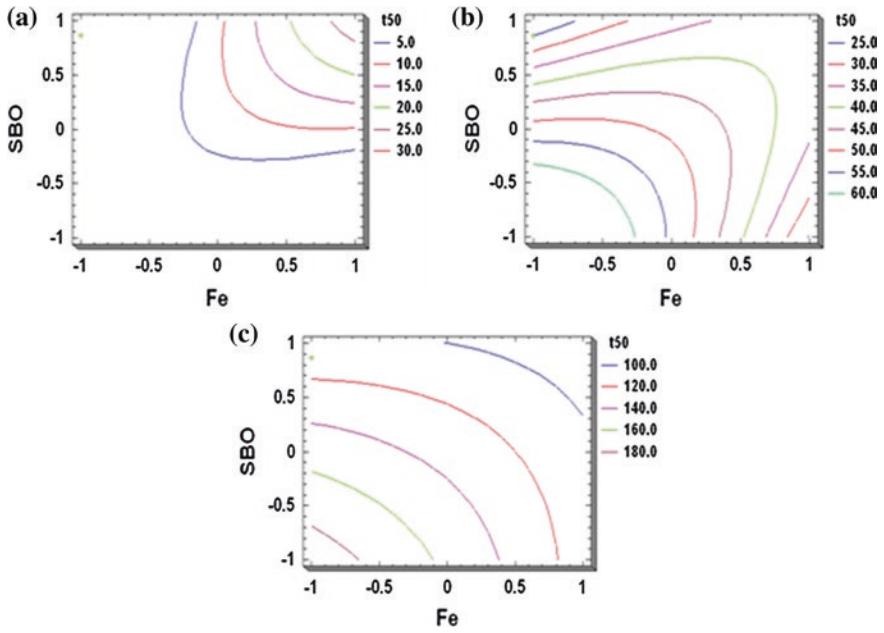

Fig. 5.1 Contours of the estimated response surfaces for the half-life time (t_{50}, min) at: **a** pH = 3; **b** pH = 5 and **c** pH = 7; where Fe and SBO represent the codified factors

5.3.1.2 Artificial Neural Network Model

The results of the Doehlert design were used to fit an artificial neural network (ANN) model with one hidden-layer feed-forward and sigmoidal response function, as presented in Fig. 5.2. The input variables were $[Fe^{3+}]_0$ (1–15 mg L^{-1}), $[SBO]_0$ (5–50 mg L^{-1}), pH (3, 5 and 7) and $[H_2O_2]_0$ (61 and 244 mg L^{-1}). The model predicts the removal of SDZ at a given irradiation time. Therefore, the output variable was $[SDZ]/[SDZ]_0$. All variables were normalized. The preliminary fitting was carried out with the complete experimental data (300 input-output data pairs) by varying the number of neurons in the hidden layer (NH) from 4 to 8 and with a total of 10,000 iterations. As a result, outliers could be identified and eliminated from the experimental data by comparing predicted values with experimental data. A fraction of ca. 25 % of the data pairs was used in the test set (TS).

The best configuration corresponds to a neural network with 7 neurons in the hidden layer, as observed in Fig. 5.2a. The agreement between experimental and calculated values is good for both data sets (Fig. 5.2b), with $\alpha = 0.999$ and 0.993 and $R^2 = 0.983$ and 0.974 for the learning set (LS) and test set (TS), respectively. Figure 5.2c shows the relative importance of the variables based on the holdback input parameter randomization (HIPR) method proposed by [11]. As expected for the photo-Fenton process, initial pH showed the largest effect upon the SDZ removal, while $[Fe^{3+}]_0$, $[SBO]_0$ and $[H_2O_2]_0$ had similar effects. Simulations of selected experiments (experiments 6, 7 and 12 of the Doehlert design) were compared with

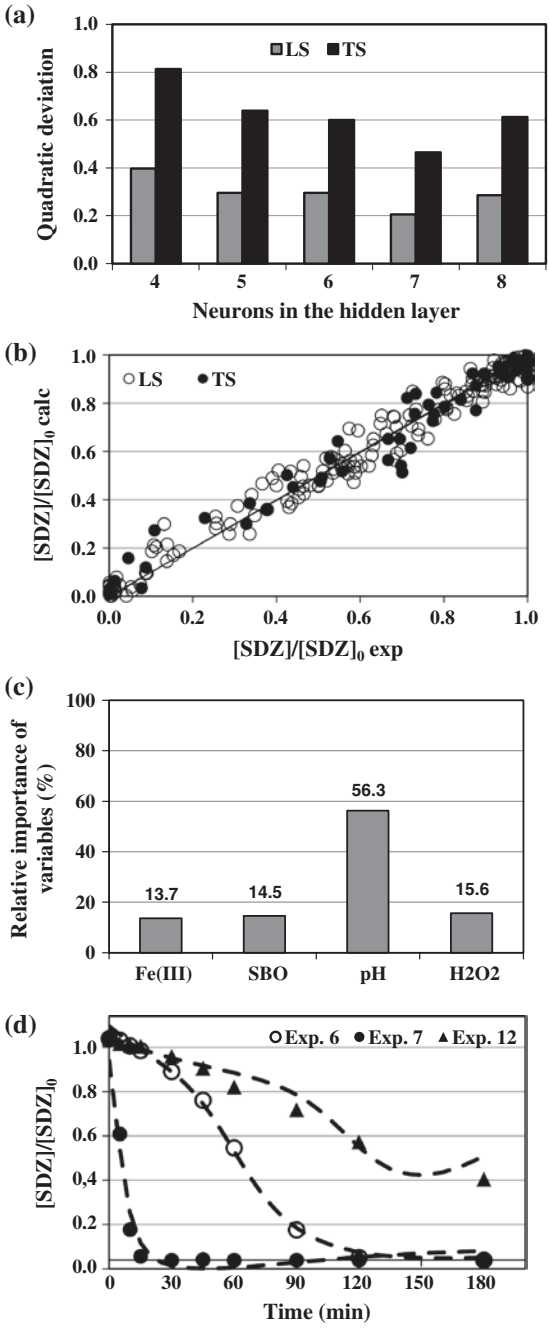

Fig. 5.2 Artificial neural network model fitting for the photo-Fenton degradation of SDZ in the presence of SBO. In 4d, *dotted lines* represent the predicted time-concentration profiles obtained with the NN model. *LS* learning set; *TS* test set

experimental results (Fig. 5.2d), confirming the good agreement between model predictions and experimental data. The neural network technique was therefore capable of extracting the information from experimental data and reproducing the behavior of a complex system. In Fig. 5.2d an interesting issue, typical of non-phenomenological models, can be observed: for experiment 12, at the end of the experiments the model predicts that the concentration of SDZ would slightly increase.

5.3.2 Application to SBO-Magnetite Particles Adsorption

Two groups of experimental data were analyzed. First, the N_2 adsorption in SBO-magnetite was studied. The second group of experimental data is the adsorption of violet crystal in SBO-magnetite particles. The data was divided into four groups. Each group was analyzed individually with the Langmuir and Freundlich equations.

5.3.2.1 Fundamentals of Adsorption and Kinetics

In general, adsorption is studied for heterogeneous kinetics and its fundamentals are widely known. Brunauer et al. [12] proposed five types of adsorption isotherms: (1) type 1: characterized by a monotonic approach to a limiting amount of adsorption, (2) type 2: it is a typical example of physical adsorption, and can occur by capillary and pore condensation; (3) type 3: it has a monotonic approach but there is not a final limit value, i.e., no saturation; (4) type 4: it is very similar to type 2, but presents a limit value; (5) type 5: it is very similar to type 3, but presents a limit value as well.

Type 1 can be modeled using the Langmuir approach:

$$v = \frac{v_m K P_A}{1 + K P_A} \tag{5.4}$$

where v_m is the volume of the monolayer, P_A is the partial pressure of species A and K is an equilibrium constant.

The Freundlich equation is:

$$Q_e = K_F C_e^n \tag{5.5}$$

Another approach is the BET model:

$$\frac{x}{v(1-x)} = \frac{1}{v_m c} + \left(\frac{c-1}{v_m c}\right)x \tag{5.6}$$

However, Eq. (5.5) cannot be used to model multilayers. Hill [13] presents an equation that may be used to estimate the number of layers:

$$v = \frac{v_m c\, x[1 - (n+1)x^n + nx^{n+1}]}{(1-x)[1 + (c+1)x - c\, x^{n+1}]} \tag{5.7}$$

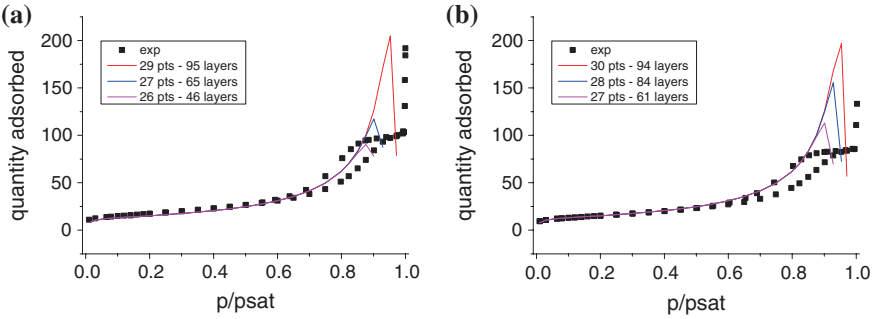

Fig. 5.3 Quantity of N_2 adsorbed (cm^3/g STP) versus pressure in BOS and magnetite **a** BOS = 0.05 mg/L; **b** BOS = 0.5 mg/L

5.3.2.2 N_2 Adsorption in SBO-Magnetite—BET

Figure 5.3 presents the adsorption isotherm of N_2 in SBO-magnetite of three different compositions corresponding to different proportions of SBO (called 0.05, 0.1 and 0.5 mg of SBO). More results can be found elsewhere [14]. Isotherms are of type 2, and the hysteresis effect points out to condensation into the pores.

The linear form of the BET equation can be used, since p/p_0 is less than 0.3. The fit can be considered adequate, because the correlation coefficients are about 0.999 (Table 5.3). The surface area was also calculated from the fit of the linearized equation by linear regression. The values are very similar to the previous ones [13]. The software used by the author is Microsoft Excel®.

The number of multilayers was estimated by adjusting Eq. (5.7). As this model is nonlinear, a nonlinear regression algorithm was used. The ESTIMA program was employed, and a likelihood function was minimized [15]. The results for two adsorption curves can be appreciated in Fig. 5.3a, b. The algorithm used here allows the estimation of the number of layers. It is about 95 for 0.05 mg particles, between 61 and 84 for 0.1 mg, and about 81 for 0.5 mg.

5.3.2.3 Adsorption of Violet Crystal in SBO-Magnetite Particles

The original data was divided into four groups that can be viewed in Fig. 5.4. The isotherms are type 1 and Langmuir and Freundlich equations are applied.

Table 5.3 Results of linear regression using the BET equation

SBO	C	v_m	R^2	S (m^2)	S (m^2)*
0.5	123.06	7.867	0.99986	34.2	34
0.1	155.82	12.47	0.99989	54.2	55
0.01	173.58	14.22	0.99992	61.6	63

*Results of Allera [14]

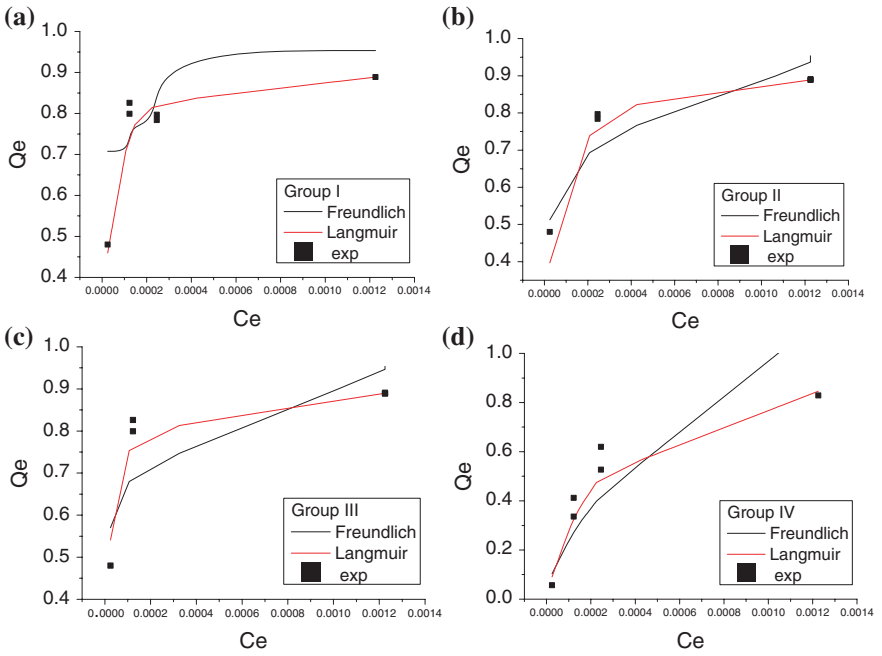

Fig. 5.4 Adsorption isotherms of violet crystal in SBO-Fe_3O_4: **a** 150 I, **b** 150 II, **c** 150 III, **d** 1000

Table 5.4 Results for the linear regression of the Langmuir equation [14]

Group	K_L	a_L	R^2
150 I	28,670	31,426	0.99993
150 II	38,054	41,990	0.99984
150 III	55,111	61,095	0.99999
1000	4,050	3,970	0.98785

The experimental data groups are fitted by the linearized Langmuir equation—see correlations in Table 5.4, but could not be fitted by the Freundlich equation. The Microsoft Excel® worksheet was used for this task and the correlation coefficients are presented in Table 5.4.

The values obtained by nonlinear regression, calculated by the software ESTIMA, for the Freundlich equation are shown in Table 5.5. In Table 5.6 the results obtained by fitting the nonlinear form of Langmuir equation are presented. The parameters are different from those calculated by linear regression (Table 5.4) but their plots are very similar (Fig. 5.5). This may be a symptom of overparameterization of the Langmuir equation for the representation of a group of data alone. The fit of a combination of groups of data was impossible with both the models, which denotes that Langmuir and Freundlich models are inadequate for the representation of the phenomenon, when considering all the data available.

Table 5.5 Results of nonlinear regression of the Freundlich equation

Group	K_L	n	R^2
150 I	2.602	6.53	0.9575
150 II	2.273	7.71	0.8376
150 III	2.247	7.73	0.8389
1000	68.11	1.63	0.9064

Table 5.6 Results of the non linear regression of Langmuir equation

Group	K_L	a_L	R^2
150 I	45,555	50,791	0.9123
150 II	40,489	45,662	0.9063
150 III	44,004	50,878	0.9028
1000	10,050	16,012	1.0000

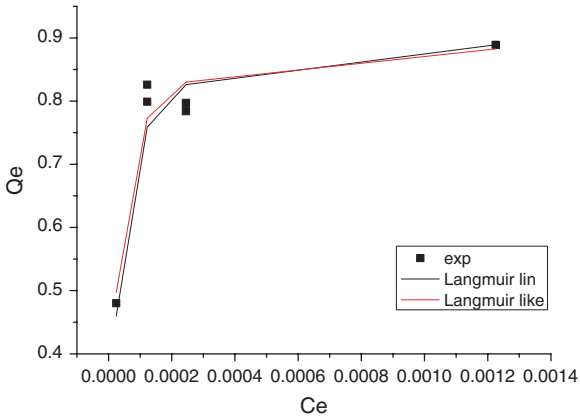

Fig. 5.5 Comparison between linear and non linear parameter estimation. Isotherms adsorption of crystal violet in SBO–Fe_3O_4 (150 mg/L—group I)

The algorithm used here is able to estimate the number n of the N_2 layers adsorbed in BOS and magnetite. The experimental data of violet crystal adsorption in Fe_3O_4 and BOS were fitted by the linearized Langmuir equation, but not by the linearized Freundlich equation. The values of the violet crystal adsorption on Fe_3O_4 and BOS estimated by nonlinear regression are different from those calculated by the linear fit, but the plots are very similar, which may point out to overparameterization of the Langmuir model for the representation of a data group alone. Fitting the data altogether by a unique model was impossible, thus other mechanisms should be studied for this purpose.

5.4 Conclusions

Mathematical modeling for SBO applications was introduced in this chapter. An overview of the theoretical background was given in the introduction. Linear regression was illustrated by the use of surface response technique and by the fit

of linearized forms of adsorption models. Nonlinear regression was illustrated by the application of BET, Langmuir and Freundlich models. The application of Overparameterization models was exemplified by the application of an artificial neural network model. The main concerns and characteristics of all the modeling techniques could be exemplified by the case studies presented.

References

1. Bard, Y. (1974). *Nonlinear parameter estimation*. New York: Academic Press.
2. Box, G. E. P., Hunter, J. S., & Hunter, W. G. (2005). *Statistics for experimenters: Design, innovation and discovery* (2nd Ed). Wiley-Interscience, Hoboken.
3. Walter, E., Pronzato, L. (1997). *Identification of parametric models from experimental data*. Berlin: Springer.
4. Ljung, L. (1999). *System identification: Theory for the user* (2d ed.). N.J.: Prentice-Hall Inc.
5. Graciano, J. E., Mendoza, D. F., & Le Roux, G. A. C. (2014). Performance comparison of parameter estimation techniques for unidentifiable models. *Computers and Chemical Engineering, 64*, 24–40.
6. Holm, J. V., Rugge, K., Bjerg, P. L., & Christensen, T. H. (1995). Occurrence and distribution of pharmaceutical organic-compounds in the groundwater downgradient of a landfill (Grindsted, Denmark). *Environmental Science and Technology, 29*, 1415–1420.
7. Pignatello, J. J., Oliveros, E., & Mackay, A. (2006). Advanced oxidation processes for organic contaminant destruction based on the Fenton reaction and related chemistry. *Critical reviews in environmental science and technology, 36*, 1–84.
8. Gomis, J., Vercher, R. F., Amat, A. M., Mártire, D. O., González, M. C., Bianco Prevot, A., et al. (2013). Application of soluble bio-organic substances (SBO) as photocatalysts for wastewater treatment: Sensitizing effect and photo-Fenton-like process. *Catalysis Today, 209*, 176–180.
9. Avetta, P., Bianco Prevot, A., Fabbri, D., Montoneri, E., & Tomasso, L. (2012). Photodegradation of naphthalene sulfonic compounds in the presence of a bio-waste derived sensitizer. *Chemical Engineering Journal, 197*, 193–198.
10. Carlos, L., Mártire, D. O., Gonzalez, M. C., Gomis, J., Bernabeu, A., Amat, A. M., & Arques, A. (2012). Photochemical fate of a mixture of emerging pollutants in the presence of humic substances. *Water Research, 46*, 4732–4740.
11. Kemp, S. J., Zaradic, P., & Hansen, F. (2007). An approach for determining relative input parameter importance and significance in artificial neural networks. *Ecological Modelling, 204*, 326–334.
12. Brunauer, S., Deming, L. S., Deming, W. E., & Teller, E. (1940). On a theory of the van der waals adsorption of gases. *Journal of the American Chemical Society, 62*, 1723–1732.
13. Hill, C. G. (1977). *Introduction to chemical engineering kinetics and reactor design*. Hoboken: Wiley.
14. Allera, A. (2012). *Sviluppo e Caratterizzazione di Materiali Magnetici Ibridi per Abbattimento di Inquinanti in Soluzione*, tesi di laurea, Dipartimento di Chimica, Facolta' di Scienze MFN, Università di Torino, Italia.
15. Pinto, J. C. (1993). *Planejamento de Experimentos para Tratamento de dados e Controle de Qualidade*. Salvador, Bahia: SOLEQ.